Neopentane-Based Tripodal CpL_2 Ligands: Synthesis and Reactions of $CH_3C(CH_2\text{-}\eta^5\text{-}C_5H_4)(CH_2\text{-}\eta^1\text{-}PPh_2)_2RuCl$; Hindered Rotation of Vinylidene Ligands

Katrin Urtel,[a] Axel Frick,[a] Gottfried Huttner,*[a] Laszlo Zsolnai,[a] Peter Kircher,[a] Peter Rutsch,[a] Elisabeth Kaifer,[a] and Albrecht Jacobi[a]

Dedicated to Prof. Helmut Werner on the occasion of his 65th birthday

Keywords: Tripod ligands / Hindered rotation of vinylidene ligands / $CpML_2$ chelate ligands / Ruthenium / Carbenes / Carbene-type ligands / Cyclic voltammetry

The tripodal ligand $[CH_3C(CH_2C_5H_4)(CH_2PPh_2)_2]^-$ reacts with $RuCl_2(PPh_3)_3$ to produce $CH_3C(CH_2\text{-}\eta^5\text{-}C_5H_4)(CH_2\text{-}\eta^1\text{-}PPh_2)_2RuCl$, [*tripod*$CpL_2RuCl$], **1**. Complex **1** undergoes substitution of the chlorine function with various nucleophiles L′ to produce [*tripod*CpL_2RuL']$^+$. The carbonyl derivative (L′ = CO) **2**, isonitrile (L′ = RNC) **3**, nitrile compounds (L′ = RCN) **4**, and a tolane adduct (L′ = η^2-PhC≡CPh) **5** are obtained when **1** is treated with the appropriate ligands in polar solvents. Halide acceptors (e.g. $TlPF_6$) are generally needed to promote these reactions. The cyanide derivative *tripod*CpL_2RuCN (**3a**) is alkylated by $F_3CSO_3CH_3$ to give the isonitrile derivative [*tripod*$CpL_2RuCNMe$]$^+$ **3b**. Terminal alkynes HC≡CR produce vinylidene compounds [*tripod*CpL_2RuL']$^+$, where L′ = C=CHR (R = *t*Bu, **7b**; R = Ph, **7c**), or allenylidene derivatives, L′ = C=C=CPh_2 (**6**), depending on the nature of R (R = CPh_2OH for synthesis of **6**). Trimethylsilylacetylene gives the parent vinylidene species, L′ = C=CH_2 (**7a**), which is transformed to the Fischer-type carbene compound, L′ = C(OMe)Me (**8**), upon treatment with methanol. The vinylidene species **7** are deprotonated by NaOMe to produce the alkynyl compounds *tripod*$CpL_2RuC{\equiv}CR$ (**9**). Methylation of **9** with $F_3CSO_3CH_3$ results in the vinylidene derivatives L′ = C=C(Me)R (R = *t*Bu, **7d**; R = Ph, **7e**), having two organic substituents at the terminal carbon centre. For all vinylidene compounds with two different substituents at their terminal carbon atom, hindered rotation of the single-faced vinylidene π-ligand about its Ru–C bond is observed. Analysis by ^{31}P-NMR spectroscopic coalescence measurements as well as line-shape analyses reveals activation enthalpies of around 40 kJmol^{-1} for this rotation, with small activation entropies of around ±10 Jmol^{-1}K^{-1}. Solid-state structures of nine compounds of the type [*tripod*CpL_2RuL']$^{+n}$ (n = 0, 1) demonstrate the remarkable conformational rigidity of the *tripod*CpL_2Ru template. They also show that the possible strain imposed by linking the Cp ligand and the two donor groups L in one and the same chelate scaffolding does not appear to impose a serious steric strain on these templates.

Introduction

$CpML_2$ compounds have played an important role in the development of organometallic chemistry as a tool for organic synthesis.[1] The $CpFe(CO)_2$ template and the $CpFeL_2$ species have been extensively studied[2] with regard to their interactions with organic substrates and many organic transformations mediated by this type of template have been reported.[2][3] Many of the organometallic derivatives that are rather unstable with $CpFeL_2$ as the organometallic group, making them non-isolable, are comparatively stable with the $CpRuL_2$ fragment as the organometallic moiety. Accordingly, there is a considerable volume of literature concerning the structure and properties of organic derivatives of the $CpRuL_2$ template.[3][4]

An inherent problem in the stereochemical interpretation of the reactions of such templates is the potential non-rigidity of $CpML_2$ fragments.[3−6] Quite early on in their seminal contributions, Brunner et al.[3][6] demonstrated that in the course of a reaction, CpMLL′ templates (M = Mn, Fe) may undergo inversion of configuration in a process geometrically similar to the inversion of ammonia. This type of behaviour tends to reduce the applicability of such CpMLL′ templates in diastereoselective organic transformations.

It thus appears that $CpML_2$ templates in which this type of configurational instability is prevented through appropriate design of the ligands might be of some use for the further development of this branch of chemistry. An appropriate design would impose a geometrical constraint upon the mutual positions of the Cp and L donors. Such a constraint is inherent in tripodal ligands, where the three donor groups, the Cp residue, and the L donors are bridged by a covalent framework. If the covalent linkers are sufficiently short, inversion of such a $CpML_2$ entity, once formed, becomes geometrically impossible.

As part of a strategy centred on the synthesis of a wide variety of neopentane-based tripod ligands $CH_3C(CH_2X)(CH_2Y)(CH_2Z)$ (X, Y, Z = donor groups), ligands of the

[a] Anorganisch Chemisches Institut der Universität Heidelberg, Im Neuenheimer Feld 270, D-69120 Heidelberg, Germany
Fax: (internat.) +49 (0)6221/545707

  1434−1948/00/0101−0033 $ 17.50+.50/0

type $[CH_3C(CH_2C_5H_4)(CH_2PR_2)(CH_2PR'_2)]^-$ have been prepared.[7] It was shown that this type of ligand is capable of producing $CpML_2$ entities (M = Mn, Mo, Fe, Co) with the Cp residue and the phosphorus donor entities linked via the neopentane framework.[7][8]

In this paper, we report on the synthesis of a variety of compounds containing the $CH_3C(CH_2C_5H_4)$-$(CH_2PPh_2)_2Ru$ template. Derivatives of this template incorporating nitrile, isonitrile, carbene, vinylidene, and allenylidene moieties, amongst others, are described. Their mutual transformations as well as their structures and redox properties are discussed. The dynamic behaviour of the corresponding vinylidene species is analysed.

Results and Discussion

1. Synthesis of $CH_3C(CH_2$-η^5-$C_5H_4)$-$(CH_2$-η^1-$PPh_2)_2RuCl$ (1)

The ligand $CH_3C(CH_2C_5H_4)(CH_2PPh_2)_2Li$ is accessible from $CH_3C(CH_2OH)_3$ in a few steps.[7] It had previously been observed that its tripodal coordination to metals may necessitate some specialized reaction procedures in order to avoid the formation of coordination polymers as well as of Cp_2M compounds.[7][8] Thus, it was not surprising that reaction of $RuCl_3 \cdot n\,H_2O$ with the ligand in ethanol, which represents a standard protocol for the preparation of $Cp(PPh_3)_2RuCl$,[9] did not work with the tripodal ligand. Either no reaction or decomposition of the ligand was observed under these conditions.

Using $RuCl_2(dmso)_4$ as the starting material[10] was found to lead to the desired *tripod*CpL_2RuCl compound **1**, albeit only in small yields [$CH_3C(CH_2C_5H_4)(CH_2PPh_2)_2Ru$ will henceforth be abbreviated as *tripod*CpL_2Ru]. It was eventually found that $RuCl_2(PPh_3)_3$, prepared from $RuCl_3 \cdot n\,H_2O$ and PPh_3 in methanol,[11] reacts with [*tripod*CpL_2]$^-$ in 1,2-dichloroethane (DCE) at 90°C to produce a fair yield of **1**.

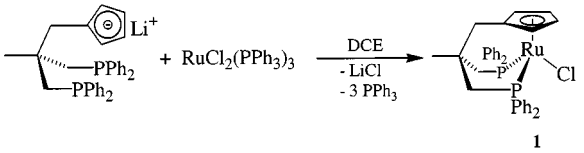

1

Chromatographic separation of **1** from PPh_3 on Al_2O_3, using diethyl ether/CH_2Cl_2 as the mobile phase, gives the desired product in yields of up to 60%. The identity of **1**, already apparent from its analytical and spectroscopic data (Table 8), was further corroborated by its X-ray analysis (Figure 1; Tables 4, 5, and 7).

The primary reason for analyzing the structure of **1** was, however, to gain insight into the steric encumbrance imposed on the $CpML_2$ entity by the fixed tripodal arrangement of its ligand constituents.

Figure 2b shows a spacefilling model of **1**, which indicates that the chlorine function is well protected by the constituents of the ligand. For comparison, the spacefilling model of $Cp[PPh_2CH(CH_3)CH_2PPh_2]RuCl$[12] is shown in Figure 2a. It is evident that in this compound, where there is no covalent link between the Cp group and the diphosphane ligand, the PPh_2 groups adopt a different orientation that makes the chlorine function more accessible. It therefore seems likely that associatively initiated reactions should be problematic with **1**, while dissociative initiation, i.e. removal of the chlorine in a first step, might well be favorable. In this respect, it is interesting to compare **1** with $Cp(PPh_3)_2RuCl$[13] (Figure 2c). The potentially reactive chlorine position appears to be even less accessible in the latter PPh_3 derivative as compared to **1** (Figure 2b). Nevertheless, $Cp(PPh_3)_2RuCl$ has in fact been found to be quite reactive with respect to chlorine substitution. A reaction of $Cp(PPh_3)_2RuCl$ initiated by an associative process is difficult to imagine (Figure 2c). Dissociative activation of this compound might, however, follow from PPh_3 as well as from Cl^- dissociation, which may account for its reactivity.[13] Dissociative activation of **1** by cleavage of one of the M−P bonds should be largely disfavoured by the chelate nature of the ligand. It thus appears that the only low energy pathway leading to chlorine substitution in **1** should

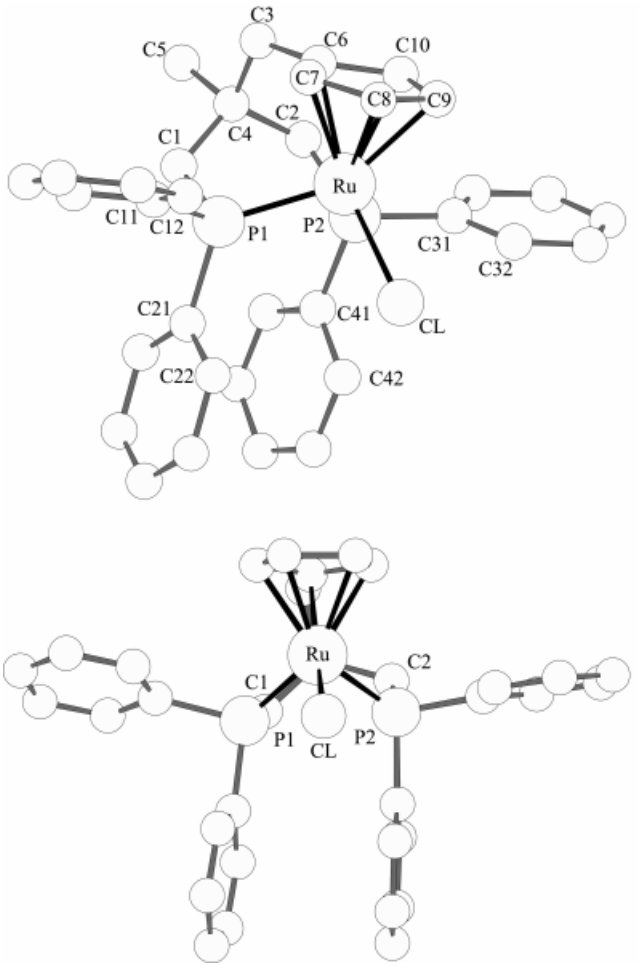

Figure 1. The structure of **1** in two different projections: top − general view; bottom − view along the Ru−C4 axis (the labelling scheme adopted for atoms of the tripodal ligand, as shown here for **1**, is consistently used for all structures reported in this paper)

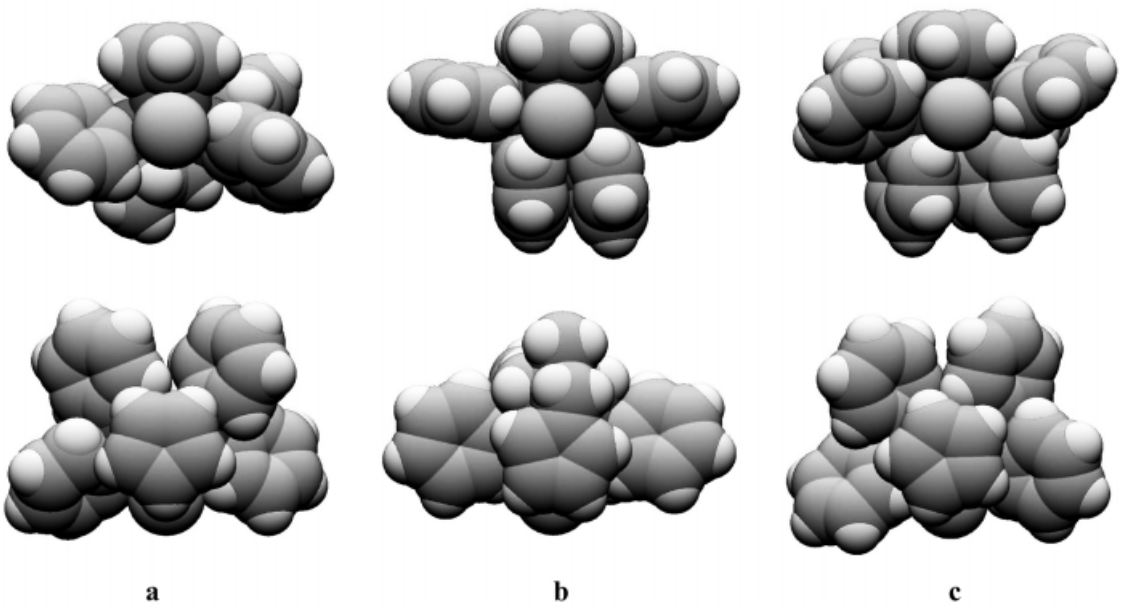

Figure 2. Spacefilling models of CpL_2Ru compounds as seen along the Cl−Ru axis (top) and in a projection onto the Cp planes (bottom); a: $Cp[PPh_2CH(CH_3)CH_2PPh_2]RuCl$; b: **1**; c: $Cp(PPh_3)_2RuCl$

be that involving heterolytic cleavage of the Ru−Cl bond. Bearing this in mind, the optimum conditions for substituting the chlorine function in **1** should be realized by using polar solvents and by carrying out the reactions in the presence of halide acceptors. In this way, a series of transformations of **1** has been achieved.

2. Substitution Reactions of 1

The cationic carbon monoxide derivative **2** is obtained when a solution of **1** in CH_2Cl_2 is treated with $TlPF_6$ under CO at 1 bar.

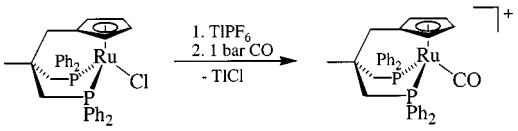

1 **2**

Analytically pure $\mathbf{2} \cdot PF_6$ can subsequently be isolated as a yellow microcrystalline powder (Table 8). Its $\tilde{\nu}_{CO}$ absorption is observed at 1966 cm^{-1}, in the region characteristic for $[CpL_2RuCO]^+$ compounds.[14] The pattern of NMR signals observed for the coordinated *tripod*CpL_2 ligand (Table 8) unequivocally proves its identity. The ^{31}P-NMR resonance is observed at $\delta = 45.3$. ^{13}C-NMR resonances are observed for all the individual carbon atoms of the ligand as well as for the coordinated CO group (Table 8).

Due to the rigid chelate framework, there are two distinct types of phenyl groups. Figure 2b (top) clearly shows these two classes: with respect to an idealized C_s symmetry (vertical mirror plane in Figure 2b), two phenyl groups, one at each of the two phosphorus nuclei, lie closely parallel to this plane. The remaining two phenyl groups are closely parallel to one another and lie in a "horizontal" plane at right angles to the idealized mirror plane. The *ipso* carbons of these two classes of phenyl residues give rise to two distinct NMR signals, which appear as pseudo triplets due to ^{31}P coupling. The carbon atoms in the *para* position show no apparent ^{31}P coupling. The pattern due to the carbon atoms of the coordinated cyclopentadienyl system is clearly resolved (Table 8).

In the ^1H-NMR spectrum, the Cp protons show the expected AA′XX′ pattern. The methylene protons of the CH_2 groups bonded to phosphorus give rise to two distinct doublets in the $^1H\{^{31}P\}$-NMR spectrum, while the CH_2 group linked to the Cp entity is seen as a broad singlet (Table 8). These NMR spectroscopic observations are in agreement with analogous findings reported for other compounds containing the same type of *tripod*CpL_2 ligand.[7][8] The same general features of the NMR spectra of **2**, as discussed above, also hold true for the other ruthenium derivatives of the same ligand described in this paper. The relevant data are collected in Tables 8−13 (Experimental Section); in the following paragraphs the discussion will be limited to references to these tables, except for compounds **7a−e**, where dynamic processes are observed.

1 reacts with KCN in methanol to produce **3a**, which is obtained as a yellow microcrystalline powder in analytically pure form after chromatographic workup.

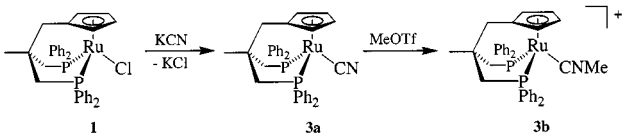

1 **3a** **3b**

The identity of **3a** was confirmed by its spectroscopic data (Table 8) as well as by an X-ray analysis (Figure 3; there are two crystallographically independent species **3a** in

the crystal, only one of which is depicted in Figure 3; Tables 4, 5, and 7).

As a derivative of **3a**, the isonitrile compound **3b** was obtained by treating **3a** in CH_2Cl_2 with $F_3CSO_3CH_3$. The triflate salt of **3b**, obtained as a pale-yellow powder, has been fully characterized (Table 9) by its spectroscopic and analytical data.

When methanolic solutions of **1** are treated with isonitriles, substitution does not take place spontaneously. Only when $TlPF_6$ is added to these solutions is complete substitution observed.

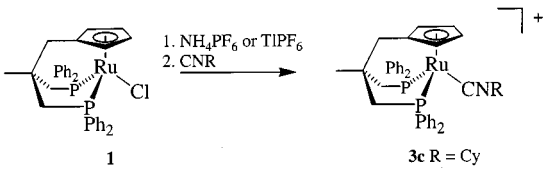

1 **3c** R = Cy

Instead of $TlPF_6$, NH_4PF_6 may also be used as an activator. The PF_6 salt of **3c** is obtained as a pale-yellow powder in analytically pure form, with all the spectroscopic data being consistent with the given constitution (Table 9). As is often found for isonitrile derivatives, the ^{13}C-NMR signal of the isonitrile carbon cannot be detected[15] while the signals of all the other carbon atoms are clearly evident (Table 9).

The chlorine function in **1** may also be replaced by nitriles.

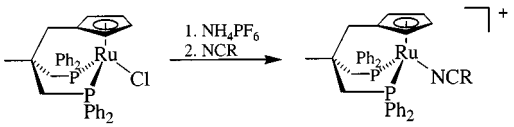

1 **4a** R = Me
4b R = Ph

A methanolic solution of **1** reacts smoothly with acetonitrile in the presence of NH_4PF_6 to produce the PF_6 salt of **4a**. The benzonitrile derivative **4b** is accessible by the same type of procedure. Compounds **4** are obtained as yellow microcrystalline salts and have been fully characterized by their spectroscopic and analytical data (Tables 9 and 10). X-ray analysis of **4b** · PF_6 leaves no doubt as to its constitution (Figure 3; Tables 4, 5, and 7).

The substitution reactions of **1** leading to **2**–**4** are analogous to corresponding reactions in the chemistry of conventional CpL_2Ru compounds, i.e. compounds where the Cp ligand is not covalently linked to the donor groups L.[14–16] It appears that chlorine substitution in **1** is not drastically impeded by the reduced flexibility of the cage-type *tripod*CpL_2Ru template. This is an important observation with regard to the analysis of the reactivity of **1** towards alkynes, since all of the many transformations known for the system CpL_2Ru/alkyne necessarily start with a substitution reaction.

3. Transformation of Alkynes by the *tripod*CpL_2Ru Template

Solutions of **1** in CH_2Cl_2 react with 1,2-diphenylacetylene when the reaction mixture is activated with $TlPF_6$. Substitution of the chlorine function of **1** by the alkyne function is a slow process requiring many hours at 25°C to reach completion.

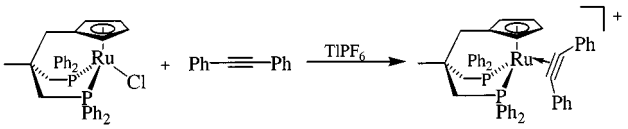

1 **5**

The PF_6 salt of **5** is obtained as an orange-yellow powder. Crystals may be obtained by slow diffusion of diethyl ether into DCE solutions of **5** · PF_6. The constitution of the compound has been verified by HR-FAB analysis (see Experimental Section, Table 14) and NMR spectroscopy (Table 10), and furthermore by an X-ray structure determination (Figure 3, Tables 4, 5, and 7). Despite the fact that the determined structure is not very accurate, due to the rather poor quality of the crystals obtained, the constitution of **5**·PF_6 is clear beyond doubt (Figure 3). The rotational orientation of the alkyne entity relative to the *tripod*CpL_2Ru template is close to orthogonal to the idealized mirror plane (Figure 3) and thus corresponds to the geometry anticipated by MO reasoning.[17] The length of the coordinated C–C triple bond (127.2 pm) as well as the bond angles C(alkyne)–C(alkyne)–C_i(phenyl) (148.1°, 147.8°) fall within the ranges normally observed for η^2-bonded alkynes.[18] It appears that the phenyl substituents at the alkyne ligand and the horizontal pair of phenyl substituents at the phosphorus centres are subject to some interference, which is manifested in a torsional position of the latter phenyl groups significantly different from the average (Figure 3; Tables 4 and 5).

Whenever terminal alkynes are reacted with a CpL_2Ru precursor, rearrangements tend to occur.[19] Although it has always been thought highly probable that the first step in such reactions is again η^2-coordination of the alkyne,[20] this has only recently been proved to be the case.[19–21] Mechanistic alternatives based on oxidative addition with C–H bond cleavage as the first step have also been proposed[20,22,23] and have in fact been verified with templates other than $CpRuL_2$.[23][24] For $CpRuL_2$, theoretical reasoning[20] tends to disfavour this latter hypothesis[20–24] and the observation that η^2-coordination does in fact occur gives additional credit to the suggestion that the transformation undergone by alkynes HC≡CR at $CpRuL_2$ templates involves η^2-coordination of the alkyne as the first step.

Since the characterization of **5** shows that the *tripod*CpL_2Ru template is capable of η^2-bonding of alkynes, alkynes HC≡CR can be expected to undergo transformations similar to those that have been observed with traditional $CpRuL_2$ entities.[19]

One of the standard transformations mediated by $CpRuL_2$ templates is the generation of allenylidene ligands

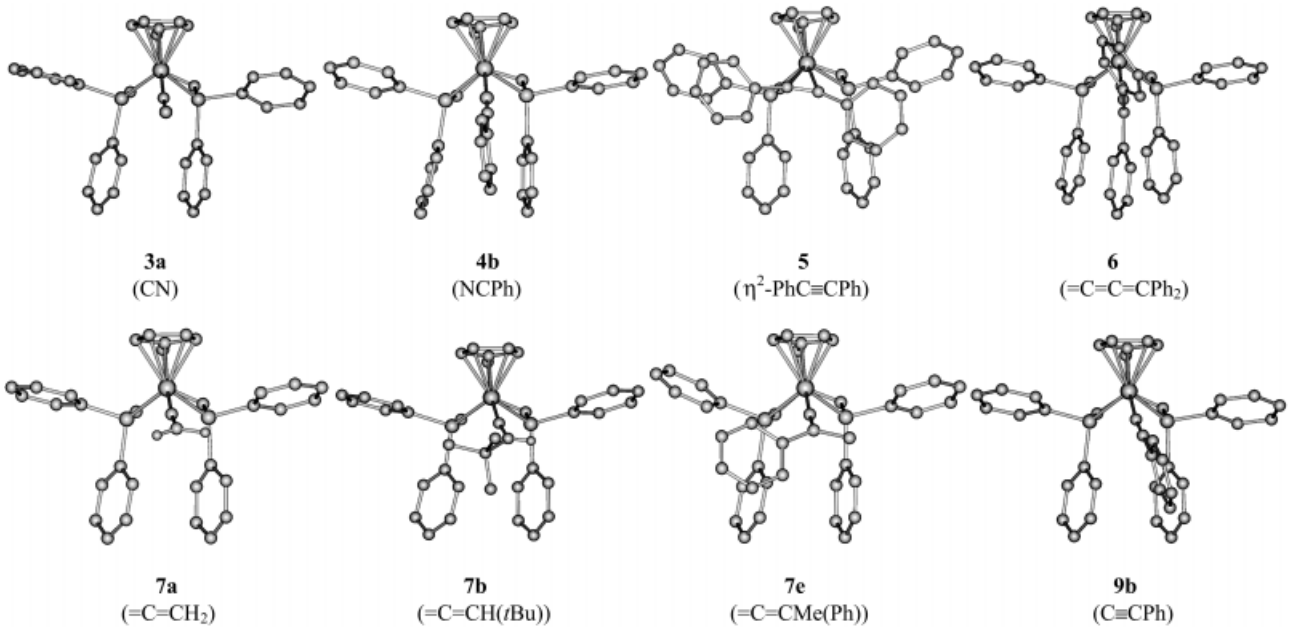

Figure 3. X-ray structures of compounds **3−9**; view along the Ru−C4 axis; coligands are shown in brackets

from $HC{\equiv}C{-}CR_2OH$.[25] This type of transformation is found to proceed equally well with *tripod*CpL_2Ru as the template. An orange suspension of **1** in methanol containing NH_4PF_6 reacts with $HC{\equiv}C{-}CPh_2OH$ to produce a purple solution of **6**, the PF_6 salt of which can be isolated as a microcrystalline purple solid.

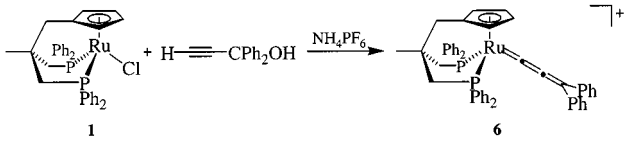

A correct elemental analysis and the spectroscopic signature of **6** (Table 10) leave no doubt as to its identity. An X-ray analysis of the PF_6 salt of **6** (Figure 3, Tables 4, 5, and 7) reveals an almost linear arrangement of the $Ru{-}C_3$ chain of the allenylidene fragment (Table 5). The coordination plane of the terminal sp^2 carbons of the ligand is almost coincident with the idealized mirror plane of the coordination polyhedron (Figure 3). The rotational position of the phenyl groups at the terminal carbon of the allenylidene ligand also tends to be close to this orientation (Figure 3).

Terminal alkynes lacking the reactive group at the γ-carbon that leads to the allenylidene ligand in **6**, produce vinylidene species **7b/c** when reacted with **1** under appropriate activation.

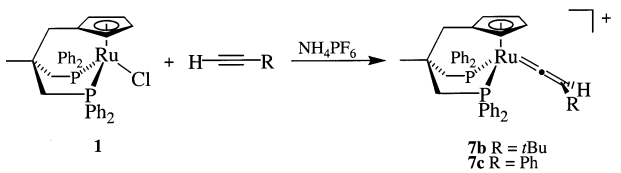

Products **7b/c** can be isolated as their PF_6 salts. Orange-brown **7b** · PF_6 and red-brown **7c** · PF_6 have been fully characterized by their analytical and spectroscopic data (Table 11). X-ray analysis of **7b**·PF_6 [Tables 4, 6, and 7; Figure 3 (there are two crystallographically independent species **7b** in the crystal, only one of which is shown in Figure 3)] shows that the orientation of the vinylidene ligand with respect to the $CpML_2$ template is such that the coordination plane about the β-carbon of the vinylidene group is "horizontal". This type of orientation is in line with expectation, considering the different π-bonding capabilities of the d-type orbitals of the $CpML_2$ unit.[17][26] The differentiation between these two π-bonding metal orbitals − that in the idealized mirror plane leading to a weaker π-interaction and the other, vertical to it, having better π-bonding capabilities − is generally not sufficient to lead to just one rigid conformation. Nevertheless, the preferred orientation, as predicted by theory,[17,19,26] is generally found to be adopted in solid-state structures. This also holds true for all the structurally characterized vinylidene compounds described in this paper. It is also the case for the allenylidene species **6** where, due to one additional carbon atom in the unsaturated chain, the sp^2 plane of the terminal carbon atom should lie within the idealized mirror plane of the template, as is indeed found (Figure 3, **6**).[17][26]

The barrier to ligand rotation imposed by this type of π-bonding has been estimated to be around 10−20 $kJmol^{-1}$ by theory,[17][26] while experimentally determined values have amounted to 29−42 $kJmol^{-1}$ for CpL_2Fe compounds[27] and to around 40 $kJmol^{-1}$ for $CpRuL_2$ compounds.[19][28] It would appear that the conformational rigidity of the *tripod*CpL_2Ru framework and the use of ^{31}P-NMR spectroscopy as the means of monitoring may allow

experimental estimation of this barrier for compounds **7**. On cooling, CD_2Cl_2 solutions of **7c** are found to show a broadening of the ^{31}P-NMR signal at $\delta = 51.4$ (178 K), such that at 170 K a splitting of this single resonance into two components ($\delta = 51.5, 51.6$) is observed (Table 1). Solubility problems prohibit analysis at lower temperatures in this case.

One sharp ^{31}P-NMR signal ($\delta \approx 51.5$) is observed for **7b** at temperatures above 178 K. Some broadening of the signal is apparent around 178 K ($\delta = 51.5$). At 159 K, two doublets are observed ($\delta = 51.4$ and 52.3; $^2J_{AB} = 45$ Hz). Coalescence occurs at 170 K ($\delta = 51.8$).

The above observations indicate that a dynamic process is operative, rendering the two phosphorus nuclei non-equivalent at low temperature while, in a dynamic sense, they are equivalent at higher temperatures. In order to further elucidate the nature of this dynamic process, the parent vinylidene compound **7a** was synthesized by reacting a suspension of **1** in CH_2Cl_2 containing $TlPF_6$ with $HC{\equiv}CSiMe_3$ to give **7a** · PF_6.

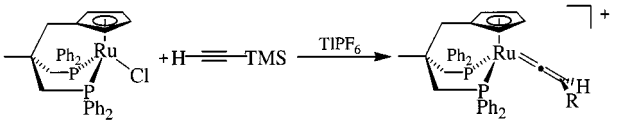

1 **7a** R = H

7a · PF_6 was isolated as a yellow microcrystalline solid and has been characterized by all the standard analytical tools (Table 11), including by an X-ray structural analysis (Figure 3; Tables 4, 6, and 7). An analogous reaction of **1** in methanol in the presence of NH_4PF_6, although initially producing **7a** (NMR control), ultimately led to the formation of the carbene compound **8**.

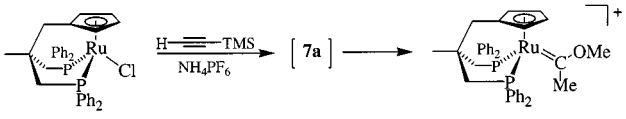

1 **8**

The transformation of vinylidene ligands into carbene ligands is not without precedence,[29] although it has been reported that in some cases the transformation is sufficiently slow to allow the isolation of the intermediate vinylidene species, even in the presence of methanol.[29b] The yellow-brown salt **8** · PF_6 has been fully characterized by a complete set of standard analytical data (Table 12).

In relation to the dynamic behaviour observed for **7b/c**, the ^{31}P-NMR spectroscopic behaviour of **7a** is of interest. If the appearance of two ^{31}P-NMR signals for **7b/c** at low temperatures were to stem from a differentiation of the surroundings of the two phosphorus nuclei by a helical twist of the chelate scaffolding − which would be dynamic at high temperatures and frozen out at low temperatures − this splitting should also be observed for **7a** (assuming that the activation barrier for the twist of the cage is largely independent of the nature of the substituents at the terminal carbon of the vinylidene ligand). It is found, however, that down to 170 K, which represents the lowest accessible temperature, the ^{31}P-NMR resonance of **7a** remains as a sharp singlet. Freezing out of the twist of the cage can therefore be ruled out as the basis of the dynamic phenomena observed for **7b/c**. Due to the symmetry of the ligand, analysis of **7a** cannot of course provide data that might allow to answer the question as to whether it is the rotation of the vinylidene ligand about its ligand−metal bond that forms the basis of the phenomena observed for **7b/c**. This question might be addressed if it were possible to slow down this rotation to such an extent that the phenomena might be observed at higher temperatures, thereby circumventing the aforementioned solubility problems. Substitution of the terminal carbon of the vinylidene unit by two different organic groups can be expected to effectively serve this purpose. With this in mind, procedures allowing the synthesis of **7d/e** were developed, which were ultimately obtained from the alkynyl species as shown.

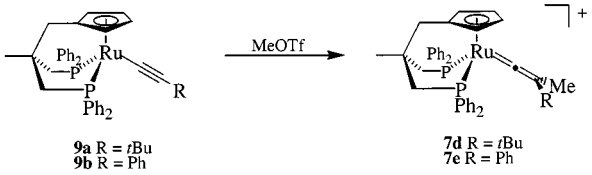

9a R = *t*Bu
9b R = Ph

7d R = *t*Bu
7e R = Ph

The alkynyl species **9a/b** are themselves available by deprotonation of the corresponding vinylidene compounds **7b/c**.

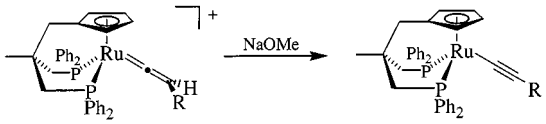

7b R = *t*Bu
7c R = Ph

9a R = *t*Bu
9b R = Ph

Compounds **9** are obtained as lemon-yellow materials of a somewhat waxy consistency. Their analytical data correspond to the depicted formulae and their spectroscopic data are in full agreement with the assigned constitutions (Table 13). X-ray analysis of **9b** gave independent confirmation of its identity (Figure 3; Tables 4, 6, and 7).

4. Model Compounds for the Analysis of Vinylidene Rotation

The alkynyl derivatives **9** are found to react smoothly with $F_3CSO_3CH_3$ as an alkylating agent in a type of reaction well-established in CpL_2Ru chemistry.[30] The triflate salts of **7d/e** are obtained as microcrystalline solids (**7d** orange-red, **7e** brick-red). Their analytical and spectroscopic data (Table 12), as well as an X-ray analysis of **7e** (Figure 3; Tables 4, 6, and 7) leave no doubt as to their constitutions. The orientation of the coordination plane of the terminal carbon of the vinylidene group is again as in **7b** (and **7a**, see above), such that this plane is vertical to the idealized mirror plane of the *tripod*CpL_2Ru template (Figure 3).

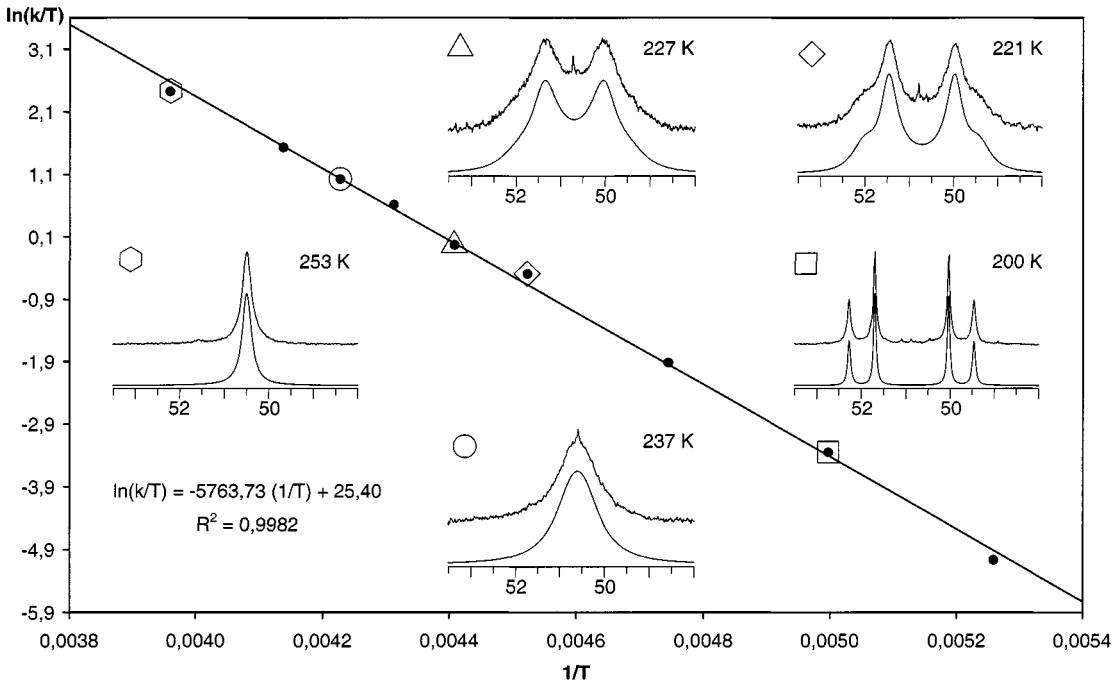

Figure 4. Eyring plot and examples of experimental (top) and simulated spectra (bottom) for compound **7e**

The ^{31}P-NMR spectrum of the triflate salt of **7e** shows one sharp signal at $\delta = 50.5$ at temperatures down to 253 K. At 242 K, significant broadening is observed, with two individual signals evolving at 227 K and a sharp pair of doublets being evident at 211 K. From the coalescence temperature of 232 K, $\Delta G^{\ddagger}_{232}$ may be estimated to be 44.5 kJmol^{-1}, corresponding to a rate constant of $k_{232} = 452$ s^{-1} (Table 1). Line shape analysis[31] of the complete set of spectra obtained at the specific temperatures given in Table 2 neatly reproduces the observed patterns (Figure 4).

The corresponding Eyring plot shows no significant deviation from linearity over the whole range of temperatures from 253 K to 190 K (Table 2; Figure 4). From this, the activation enthalpy $\Delta H^{\ddagger}$ can be estimated to be 47.9 kJmol^{-1}; $\Delta S^{\ddagger}$ is found to be 13.6 Jmol^{-1}K^{-1} (Table 2; Figure 4).

Table 1. Rotational barriers estimated from coalescence temperatures

	T [K]	P_A [ppm]	P_B [ppm]	J_{AB}[Hz]	Tc [K][a]	ΔG_{Tc} [kJ mol^{-1}]
7b	178	51.5			170	32.7[b]
	159	51.4	52.3	45		
7c	178	51.4			175	34.0[b]
	170	51.5	51.6	n.d.		
7d	253	50.3			227	43.1[b]
	200	49.8	52.0	48.6		
7e	253	50.5			232	44.5[b]
	211	49.8	52.0	48.6		

[a] Tc = coalescence temperature. – [b] $k_{Tc} = 303$ s^{-1} for **7b**; 254 s^{-1} for **7c**; 566 s^{-1} for **7d**; 452 s^{-1} for **7e**.

The same type of experiments were performed with **7d** (see data in Table 2). The fit obtained by line shape analysis[31] was equally good and the corresponding Eyring plot was again linear over the whole temperature range [$\ln(k/T) = -4849.09(1/T) + 22.3$; $R^2 = 0.9935$]. The thermodynamic data estimated from line shape analysis are given in Table 2, along with the estimates from the coalescence temperature (227 K) of k_{227} (566 s^{-1}) and $\Delta G^{\ddagger}_{227}$ (43.1 kJmol^{-1}) (see Table 1). For **7d** and **7e**, the respective $\Delta H^{\ddagger}$ values are found to be 40.3 kJmol^{-1} and 47.9 kJmol^{-1} (Table 2).

Table 2. Calculated rotational barriers and thermodynamic parameters from line shape analyses

T [K]	**7d** k [s^{-1}]	**7e** K [s^{-1}]
253	5300	2850
242	2650	1120
237	–	660
232	1025	430
227	–	220
221	340	135
211	95	31
200	24	7
190	5.5	1.2
178	2	–
Thermodynamic data	$\Delta H^{\ddagger} = 40.3$ kJ mol^{-1}	$\Delta H^{\ddagger} = 47.9$ kJ mol^{-1}
	$\Delta S^{\ddagger} = -12.12$ J mol^{-1}K^{-1}	$\Delta S^{\ddagger} = 13.60$ J mol^{-1}K^{-1}
	$\Delta G_{298}{}^{\ddagger} = 43.9$ kJ mol^{-1}	$\Delta G_{298}{}^{\ddagger} = 43.9$ kJ mol^{-1}

The activation entropies are small for both compounds (Table 2). Since a conservative estimate of the standard deviation of $\Delta S^{\ddagger}$ is around 7 Jmol^{-1}K^{-1}, the $\Delta S^{\ddagger}$ values (**7d**: $\Delta S^{\ddagger} = -12$ Jmol^{-1}K^{-1}; **7e**; $\Delta S^{\ddagger} = +14$ Jmol^{-1}K^{-1}) do not warrant a detailed discussion. However, the small magnitude of these values indicates that the steric crowding and

strain within the molecule are not subject to any great changes along the reaction coordinate.

7b/c can be thought of as analogues of **7d/e** having a hydrogen substituent at the terminal position where **7d/e** bear a methyl group. As mentioned above, the low temperature limit of the rotational exchange process cannot be reached experimentally with **7b/c**. Line shape analysis is therefore not possible for these compounds due to the fact that the shifts and coupling constants of the $P_{A/B}$ system are not experimentally accessible. From the coalescence temperatures, the parameters given in Table 1 can be deduced; the $\Delta G^{\neq}$ values at these temperatures are about 10 kJmol^{-1} smaller than the values estimated for **7d/e** at their coalescence temperatures (Table 1). Of course, this cannot be solely attributed to the steric relief caused by substituting a methyl group for a hydrogen since electronic factors are also likely to come into play.

Barriers to rotation of around 10−20 kJmol^{-1} for processes of the type analysed have been predicted by theoretical methods.[17][26] The experimental data for $CpL_2Fe{=}C{=}CRR'$ indicate barriers of 29−42 kJmol^{-1} and corresponding experiments on $CpL_2Ru{=}C{=}CRR'$ lead to activation barriers of around 40 kJmol^{-1}.[27][28] The activation barriers for the *tripod*CpL_2Ru−vinylidene compounds **7** (Tables 1 and 2) are thus in favorable agreement with the theoretical predictions as well as with data obtained for similar compounds.

5. Cyclic Voltammetry

The broad variation of the coligands in compounds **1**−**9** allows for some kind of systematic comparison of their electrochemical behaviour (Table 3).

The first four entries in Table 3 correspond to neutral species. Oxidation is reversible for the first three compounds (**1**, **9a**, **9b**) and occurs in the range 20−200 mV (SCE). The oxidation process can be attributed to the Ru^{II}/Ru^{III} redox couple, since, at least for **1** with the simple chlorine ligand, there is no other plausible explanation. Since the reversible oxidation of the two alkynyl compounds (**9a/b**) occurs in the same range as found for the chloro derivative **1**, the electrochemical process responsible for this oxidation wave should still be the reversible Ru^{II}/Ru^{III} oxidation. The organic substituents are only of secondary influence and are clearly not oxidized themselves in the potential range below 200 mV. At higher potentials, around 1100 mV, a second irreversible oxidation of compounds **9** is observed (Table 3), the probable nature of which will be discussed alongside the discussion of the redox behaviour of compounds **7** and **8** (see below).

With CN as the ligand, as in **3a**, the first oxidation is irreversible. Although comparison of this irreversible process at $E_P^A = 660$ mV with the reversible processes at $E_{1/2} \leq 220$ mV observed for **1**, **9a/b** is not strictly valid in a thermodynamic sense, the CN group would be expected to shift the oxidation potential to higher values, as is observed. The first irreversible oxidation of **3a** leads to a product that is − again irreversibly − reduced at $E_P^C = -190$ mV. The nature of this product is not known. At $E_{1/2} = 1164$ mV, a second oxidation of **3a** is observed, which is reversible. The nature of the product responsible for this signal is again unknown. It is highly improbable that this feature corresponds to the formal +IV oxidation state of ruthenium. On the other hand, the observed $E_{1/2}$ is close to that observed for the oxidation of the cationic isonitrile species **3b/c**, and hence some similar structure − possibly a coordinated CNH ligand − cannot be ruled out.

The next group of compounds comprises the cationic species **2**, **3b/c**, **4**, **5**, which, in contrast to the members of the final group, do not have carbene, vinylidene, or allenylidene ligands. The carbon monoxide derivative **2** is difficult

Table 3. Electrochemical data for compounds **1** to **9**[a]

compound	ligand	potential	$E_{1/2\ (Fc)}$	ΔE_{Fc}
1	Cl	$E_{1/2} = 220$; $\Delta E = 100$	434	132
9a	C≡C*t*Bu	$E_{1/2} = 20$; $\Delta E = 100$ $E_P^A = 1100$	436	139
9b	C≡CPh	$E_{1/2} = 132$; $\Delta E = 105$ $E_P^A = 1070$	433	143
3a	CN	$E_P^A = 660$; $E_P^C = -190$ $E_{1/2} = 1164$, $\Delta E = 97$	456	126
2	CO	$E_P^A = 1700$ $E_P^C = -2000$	393	75
3b [b]	CNMe	$E_{1/2} = 1240$; $\Delta E = 150$	438	135
3c	CNCy	$E_{1/2} = 1264$; $\Delta E = 172$	435	120
4a	NCMe	$E_{1/2} = 922$; $\Delta E = 114$ $E_P^A = 1600$	414	133
4b	NCPh	$E_{1/2} = 967$; $\Delta E = 105$	431	129
5	η^2-PhC≡CPh	$E_{1/2} = 986$; $\Delta E = 105$	413	135
6	C=C=CPh$_2$	$E_{1/2} = 1203$; $\Delta E = 119$ $E_{1/2} = -730$; $\Delta E = 106$	434	108
7a	C=CH$_2$	$E_P^A = 1410$ $E_P^C = -1765$	421	138
7b	C=CH(*t*Bu)	$E_P^A = 1330$ $E_P^C = -1920$	403	125
7c	C=CH(Ph)	$E_P^A = 1215$ $E_P^C = -1690$	418	119
7d	C=CMe(*t*Bu)	$E_{1/2} = 1187$; $\Delta E = 123$ $E_P^A = 1740$	416	142
7e	C=CMe(Ph)	$E_{1/2} = 1133$; $\Delta E = 116$ $E_P^C = -1880$	412	128
8	COMe(Me)	$E_{1/2} = 1066$; $\Delta E = 103$	442	127

[a] All potentials are given in mV vs. SCE. The data refer to a scan rate of 200 mV/s. To check the reversibility, scan rates of 50, 100, 200, 400, 600, and 800 mV/s were also applied. The square-root relationship between peak height and scan rate expected for reversible processes was observed in each case. For ease of comparison, the compounds are sorted into blocks, the order of which does not necessarily correspond to the sequence of numbers used for designating the compounds. With the exception of compound **2**, which was analyzed in CH_3CN solution, all measurements were performed in CH_2Cl_2 solution. In each case, the first line of data refers to an oxidative process. The second line, where relating to irreversible processes, refers to the anodic potential of a second oxidation wave at higher potentials. If the potential is less positive (**3a**, **2**, **7a**−**7c**) than that required for the oxidation (first line), the second line refers to the cathodic potentials of the reduction waves corresponding to the products generated by the oxidation (ECE). Only for compound **6** are both oxidation and reduction found to be reversible. For reversible processes, the separation $\Delta E = E_P^A - E_P^C$ is given, together with the ΔE_{Fc} observed in the same experiment for the electrochemically reversible ferrocene redox couple at around 430 mV. − [b] Quasi-reversible oxidation.

to oxidize and reduce. Both processes are irreversible. The isonitrile analogues **3b/c** are reversibly or quasi-reversibly oxidized at around 1250 mV. With nitriles as coligands, as in **4a/b**, reversible oxidation at somewhat lower potentials is observed.

The 1,2-diphenylacetylene derivative **5** shows a reversible oxidation at 986 mV, in the same region as observed for the oxidation of the nitrile derivatives (**4a/b**). It can be seen that oxidation of these cationic compounds occurs at markedly higher potentials than found for the neutral species of the first group. This is well in accord with expectation, since abstracting an electron from a cation clearly requires more energy than ionizing a neutral species. The relatively narrow range of oxidation potentials observed for the compounds of this group (Table 3) again points to an Ru^{II}/Ru^{III} redox process similar in nature to that inferred for compounds of the first group.

The cationic compounds **6**–**8**, containing carbene ligands, form a class of their own. Of the vinylidene species **7**, compounds **7a**–**c** show irreversible oxidations around 1200–1400 mV, while the oxidations of **7d/e** are reversible and occur at $E_{1/2}$ = 1187 mV and $E_{1/2}$ = 1133 mV, respectively. Since **7a**–**c** have at least one hydrogen atom bonded to the terminal sp^2 carbon, while in **7d/e** these positions are both blocked by organic groups, it is reasonable to assume that the presence of a hydrogen in the β-position of the coligands is responsible for the irreversibility of the oxidation process observed for **7a**–**c**. In other words, deprotonation of the oxidized species may be at the basis of the observation that first oxidations of **7d/e** are reversible while those of **7a**–**c** are not. As an indication of the plausibility of this argument, the narrow range of potentials over which the oxidations of **7a**–**e** are observed (ca. 1100 to 1400 mV) may be invoked. If the primary oxidation products of the compounds **7b/c**, $[tripodCpL_2RuC{\equiv}C(H)tBu]^{2+}$ ($\mathbf{7b}^+$) and $[tripodCpL_2RuC{\equiv}C(H)Ph]^{2+}$ ($\mathbf{7c}^+$), were to undergo deprotonation, they would be transformed into $\mathbf{9a}^+$ and $\mathbf{9b}^+$, respectively. However, these compounds are known to be irreversibly oxidized at potentials around 1100 mV (Table 3), which are lower than those needed for the oxidation of **7b** and **7c**. If a process as described for **7b/c** occurs, the signals of the redox process **9a**/$\mathbf{9a}^+$ would not be expected to be observed in the voltammogram of **7b**/$\mathbf{7b}^+$ (nor analogously signals due to **9b**/$\mathbf{9b}^+$ in the voltammogram **7c**/$\mathbf{7c}^+$) and indeed no such signals are found.

Irreversible reduction at rather negative potentials is observed for **7a/b/c/e** (−1900 to −1700 mV, Table 3) and a second irreversible oxidation is seen for **7d**. The potentials at which compounds **7d/e** are reversibly oxidized are in approximately the same region as those at which reversible or quasi-reversible oxidation of compounds **3**, **4**, **5** takes place. They are also close to the potential measured for the reversible oxidation of the carbene compound **8** (1066 mV). Thus, it is obvious that the first oxidation potentials of cationic compounds in the second group (**3**–**5**) and the third group (**7**–**8**) fall in a rather narrow range, irrespective of the broad variation in the nature of the coligands. This implies that for all these cationic species the oxidation process is adequately described by the Ru^{II}/Ru^{III} redox couple. The allenylidene compound **6** also fits into this scheme, since it shows a reversible oxidation at $E_{1/2}$ = 1203 mV (Table 3). As expected for an allenylidene species, it may also be reversibly reduced (Table 3), with the extra electron being delocalized over the cumulenic system.

Table 4. Bond lengths in compounds **1**–**9** [pm][a]

	1	**3a** [b]	**4b** · PF_6[c]	**5** · PF_6[c]	**6** · PF_6	**7a** · PF_6	**7b** · PF_6[b]	**7e** · PF_6[c]	**9b**
Ru–P1	226.47(10)	227.0(3)/227.3(3)	228.1(2)	229.9(3)	229.3(2)	229.80(12)	229.71(18)/229.44(19)	231.01(13)	225.1(1)
Ru–P2	225.65(10)	224.3(3)/225.0(3)	227.5(2)	232.3(3)	228.1(2)	228.52(13)	227.55(17)/226.54(18)	227.55(13)	224.1(1)
Ru–C6	215.4(3)	219.6(10)/219.8(9)	215.9(6)	217.8(9)	222.5(5)	222.2(4)	223.3(7)/223.2(7)	223.0(4)	220.4(4)
Ru–C7	221.1(3)	222.6(10)/221.4(9)	222.5(5)	222.0(9)	223.1(6)	223.8(4)	223.7(8)/225.1(6)	225.8(4)	222.9(4)
Ru–C8	225.6(3)	227.5(9)/225.8(9)	226.9(6)	228.5(9)	226.5(6)	227.3(4)	229.1(6)/229.3(6)	228.2(4)	226.2(4)
Ru–C9	224.3(3)	225.1(10)/224.9(9)	223.9(5)	229.6(9)	226.3(6)	226.7(4)	225.8(6)/226.5(7)	225.0(4)	224.9(4)
Ru–C10	219.4(3)	220.5(9)/223.6(9)	218.9(5)	221.4(9)	223.0(5)	224.1(4)	223.1(6)/223.5(7)	221.1(4)	223.3(4)
Ru–Z	185.0	187.8/187.1	185.8	188.4	189.2	189.2	190.1/190.3	189.3	188.0
Ru–X	245.53(10)	201.2(11)/199.3(11)	205.2(5)	[d]	190.7(6)	186.7(5)	189.4(8)/188.3(8)	186.1(5)	202.2(4)
C3–C6	149.0(4)	147.9(14)/151.2(14)	151.6(8)	150.4(13)	149.9(8)	150.4(6)	151.0(9)/150.1(9)	150.5(6)	151.2(6)
C6–C7	144.8(5)	143.4(14)/143.2(13)	143.8(8)	145.0(13)	143.4(8)	143.4(6)	142.7(9)/143.8(9)	142.6(6)	141.1(6)
C7–C8	139.1(5)	139.1(14)/139.2(14)	139.9(8)	141.5(13)	140.9(8)	142.7(6)	138.9(9)/140.9(9)	140.9(6)	142.7(6)
C8–C9	143.3(5)	143.9(14)/143.2(13)	143.2(8)	141.8(13)	141.8(8)	141.5(6)	142.3(9)/142.5(9)	142.7(6)	143.0(6)
C9–C10	141.9(5)	139.1(14)/141.4(14)	141.5(8)	140.4(13)	140.1(8)	142.4(6)	141.4(9)/141.5(10)	141.1(6)	139.6(6)
C10–C6	144.1(5)	141.9(14)/147.4(13)	142.4(8)	142.8(12)	142.0(8)	143.5(6)	142.3(9)/142.8(9)	143.7(6)	144.2(6)
X–Y	–	116.8(12)/117.4(12)	114.2(7)	[d]	127.0(8)	128.1(7)	130.1(9)/128.4(9)	132.3(6)	121.0(6)
Y–W	–	–	142.7(8)	[d]	135.8(8)	–	[d]	[d]	144.1(6)
d	10.0	7.5/6.4	9.8	12.2	5.0	5.4	6.0/5.6	4.6	5.1

[a] All hydrogen atoms were identified by X-ray methods (including those at C52 in **7**). Standard deviations in units of the least significant digit given in each case. Z represents the centre of the Cp ring; X, Y, W refer to the organic residues at Ru in the sequence Ru-X-Y-W. The numbering scheme corresponds to that used in Figure 1 throughout; *d* denotes the in-plane component of the shift of the Ru atom in the direction of the carbon atom C6 with respect to the geometric centre of the 5-membered ring; C6 is the carbon atom linking the Cp residue to the ligand scaffolding. – [b] As footnote [c] with respect to the second independent molecule. – [c] For the sake of comparison, the configuration has been inverted with respect to the deposited data. – [d] Some additional distances: **5**: Ru–C(sp) 218.4(9), 221.1(9); C(sp)–C(sp) 127.2(13); C(sp)–C(*i*-Ph) 146.1(10), 146.4(11). **6**: C(γ)–C(*i*-Ph) 149.7(6), 150.0(6). **7b**: C(β)–C(*t*Bu) 152.0(9)/152.7(9); **7e**: C(β)–C(Me) 152.4(9); C(β)–C(Ph) 148.7 (6).

Table 5. Bond angles and torsion angles in **1**–**6** [°][a]

	1	**3a** [b]	**4b** · PF_6[c]	**5** · PF_6	**6** · PF_6
P1–Ru–P2	84.40(3)	86.61(10)/86.44(10)	85.81(5)	85.56(9)	85.6(6)
P1–Ru–Z	120.4	117.3/118.5	119.3	112.9	117.1
P2–Ru–Z	117.6	119.6/118.1	116.0	118.6	116.0
P1–Ru–X	100.32(3)	99.1(3)/101.0(3)	97.8(1)	120.9(3)/94.2(3)	101.4(2)
P2–Ru–X	98.82(3)	94.7(3)/95.8(3)	98.3(1)	88.2(3)/107.1(3)	98.3(2)
Z–Ru–X	126.1	129.6/127.7	129.6	121.4/127.5	128.9
Ru–X–Y	–	175.0(9)/172.9(8)	177.8(5)	[d]	173.4(5)
X–Y–W	–	–	177.0(6)	[d]	175.9(6)[d]
C4–C1–P1–Ru	−4.3	1.1/0.3	−8.6	−4.2	3.7
C4–C2–P2–Ru	−33.8	−23.9/−23.6	−29.2	−23.7	−18.0
C4–C3–C6–Ru	−16.1	−7.1/−7.4	−15.6	−14.6	−5.4
C3–C6–C7–C8	177.7	177.3/176.3	178.2	−177.9	177.6
C3–C6–C10–C9	−177.5	−176.8/−175.9	−177.8	177.8	−177.3
C12–C11–P1–Hc1	18.78	−3.98/−1.3	16.46	45.0	17.03
C22–C21–P1–Hc1	10.82	−23.50/−21.32	0.03	37.98	−16.19
C32–C31–P2–Hc2	−0.28	−25.60/−16.21	−9.68	37.88	−13.07
C42–C41–P2–Hc2	2.19	−18.17/−16.89	−6.33	25.19	−28.12

[a] Standard deviations in units of the least significant digit given in each case. Z represents the centre of the Cp ring; X, Y, W refer to the organic residues at Ru in the sequence Ru-X-Y-W; Hc represents an auxiliary point, fixed at the phosphorus atoms such that it points towards the observer (Figure 1, bottom) and is parallel to the C4–Ru axis (Figure 1). – [b] As footnote [c] with respect to the second independent molecule. – [c] For the sake of comparison, the configuration has been inverted with respect to the deposited data. – [d] Some additional angles: **5**: C(sp)–C(sp)–C(*i*-Ph) 148.1(9), 147.8(9). **6**: C(β)–C(γ)–C(*i*-Ph) 117.1(5), 121.1(5).

6. Structural Characteristics of the *tripod*CpL_2Ru Template

The structures of nine compounds derived from the *tripod*CpL_2Ru template are shown in Figures 1 and 3, with the geometrical data being collected in Tables 4–6. The data in Table 4 shows that the distances within the *tripod*CpL_2Ru template are not significantly influenced by the coligands bound to this template. The Ru–P distances are found to range only from 224 to 232 pm (Table 4). The Ru–C_{Cp} distances fall within a range from 215 to 230 pm, while the C–C distances within the Cp residue lie between 139 and 145 pm.

The P–Ru–P angles (Tables 5 and 6) are found in the narrow range from 84° to 88°. The angles subtended at the ruthenium centre by the centre of the Cp residue and the phosphorus atoms show a similarly small degree of scatter (112 to 120°, Tables 5 and 6). The position at which the coligand is bound to the template is likewise defined by a narrow range of P–Ru–X (X = coligand; 87 to 104°) and Z–Ru–X angles (Z = centre of the Cp molecule; 126 to 132°).

The coordination polyhedron around the ruthenium centre is thus fairly constant in shape (Figure 3) and is not significantly influenced by the various types of coligands

Table 6. Bond angles and torsion angles in **7**–**9** [°][a]

	7a·PF_6	**7b** · PF_6 [b]	**7e** · PF_6 [c]	**9b**
P1–Ru–P2	86.22(5)	87.03(6)/87.71(6)	85.47(5)	86.05(4)
P1–Ru–Z	116.5	115.7/114.9	116.4	118.8
P2–Ru–Z	116.2	116.1/115.7	116.8	118.7
P1–Ru–X	103.23(15)	103.98(18)/103.86(19)	102.5(13)	101.2(1)
P2–Ru–X	96.68(15)	92.87(19)/91.9(2)	96.88(12)	91.7(1)
Z–Ru–X	128.7	130.8/132.1	129.1	129.6
Ru–X–Y	172.5(4)	172.1(5)/170.6(5)	174.4(4)	174.7(4)
X–Y–W	–	[d]	[d]	178.2(4)
C4–C1–P1–Ru	0.4	0.5/−4.6	−5.8	5.7
C4–C2–P2–Ru	−20.3	−20.6/−22.3	−25.7	−22.6
C4–C3–C6–Ru	−7.5	−4.5/−6.7	−11.4	−4.5
C3–C6–C7–C8	178.2	178.9/176.9	176.3	176.0
C3–C6–C10–C9	−178.0	−177.7/−176.8	−176.3	−175.9
C12–C11–P1–Hc1	5.31	1.16/−8.37	−18.81	13.37
C22–C21–P1–Hc1	−28.10	−32.60/−38.95	−23.79	−25.02
C32–C31–P2–Hc2	−14.61	−13.52/−14.18	−20.47	17.85
C42–C41–P2–Hc2	−26.69	−28.09/−29.55	−16.55	−25.07

[a] Standard deviations in units of the least significant digit given in each case. Z represents the centre of the Cp ring; X, Y, W refer to the organic residues at Ru in the sequence Ru-X-Y-W; Hc represents an auxiliary point, fixed at the phosphorus atoms such that it points towards the observer (Figure 1, bottom) and is parallel to the C4–Ru axis (Figure 1). – [b] As footnote [c] with respect to the second independent molecule. – [c] For the sake of comparison, the configuration has been inverted with respect to the deposited data. – [d] Some additional angles: **7b**: C(α)–C(β)–C(*i*-*t*Bu) 127.2(6)/129.1(6). **7e**: C(α)–C(β)–C(*i*-Ph) 118.9(4); C(α)–C(β)–C(Me) 121.8(4).

Table 7. Crystal data for compounds **1**−**9**[a]

Compound	**1**	**3a** · 6 $CDCl_3$	**4b** · PF_6 · 0.5 CH_2Cl_2	**5** · PF_6	**6** · PF_6 · 3 CD_2Cl_2
Formula	$C_{34}H_{33}ClP_2Ru$	$C_{35}H_{33}P_2NRu$	$C_{42}H_{38}Cl_{1.5}F_6P_3NO_{0.5}$ Ru	$C_{48}H_{43}F_6P_3Ru$	$C_{49}H_{43}F_6P_3Ru$
Molecular mass	640.060	329.580	925.89	1855.610	2357.100
Crystal system	orthorhombic	triclinic	monoclinic	monoclinic	orthorhombic
Space group	$P2_12_12_1$	$P\bar{1}$	$C2/c$	$P2_1/n$	$Pbca$
Lattice constants	a = 1063.1 (2) pm	a = 1232.2 (2) pm	a = 2616.8 (5) pm	a = 934.4 (2) pm	a = 1521.3 (3) pm
	b = 1498.2 (5) pm	b = 1816.0 (4) pm	b = 2148.1 (4) pm	b = 2441.3 (5) pm	b = 2536.4 (5) pm
	c = 1748.4 (4) pm	c = 1991.4 (4) pm	c = 1904.7 (4) pm	c = 2101.6 (4) pm	c = 2637.3 (5) pm
	α = 90.00°	α = 86.71(2)°	α = 90.00(0)°	α = 90.00(0)°	α = 90.00(0)°
	β = 90.00°	β = 78.90(1)°	β = 132.02(3)°	β = 100.38(3)°	β = 90.00(0)°
	γ = 90.00°	γ = 78.30(1)°	γ = 90.00(0)°	γ = 90.00(0)°	γ = 90.00(0)°
Cell volume	2785·10^6 pm^3	4282·10^6 pm^3	7954·10^6 pm^3	4716 × 10^6 pm^3	10176 × 10^6 pm^3
Molecular units per cell	Z = 4	Z = 4	Z = 8	Z = 4	Z = 8
Density (calculated)	1.527 g/cm^3	1.534 g/cm^3	1.546 g/cm^3	1.307 g/cm^3	1.538 g/cm^3
Measuring device	Nonius Kappa CCD	Siemens Nicolet-Syntex	Nonius Kappa CCD	Nonius Kappa CCD	Nonius Kappa CCD
Temperature	200 K	200 K	200 K	200 K	200 K
Number of reflections for cell refinement		36			
Scan range	3.6° < 2θ < 52.0°	3.1° < 2θ < 47.0°	3.8° < 2θ < 51.9°	3.9° < 2θ < 48.0°	3.1° < 2θ < 52.1°
Method	ω-scan, Δω = 1.0°	ω-scan, Δω = 0.60°	ω-scan, Δω = 1.0°	ω-scan, Δω = 1.0°	ω-scan, Δω = 2.0°
Scan speed	15 sec/frame	12° min^{-1}	20 sec/frame	18 sec/frame	10 sec/frame
Measured reflections	58132	13349	40070	73701	142716
Unique reflections	5440	12672	7630	7396	10001
Observed reflections [$I \geq 2\sigma(I)$]	4642	6929	5202	5033	5301
Number of parameters refined	297	926	504	455	543
Maximum of residual electron density	0.76 × 10^{-6} e/pm^3	1.29 × 10^{-6} e/pm^3	1.19 × 10^{-6} e/pm^3	2.54 × 10^{-6} e/pm^3	0.98 × 10^{-6} e/pm^3
Agreement factors	R_1 = 0.032	R_1 = 0.072	R_1 = 0.060	R_1 = 0.085	R_1 = 0.068
(F^2 refinement)	R_w = 0.072	R_w = 0.172	R_w = 0.177	R_w = 0.275	R_w = 0.137

Compound	**7a** · PF_6 · 1.75 CH_2Cl_2	**7b** · PF_6 · CH_2Cl_2	**7e** · OTf · CH_2Cl_2	**9b**
Formula	$C_{36}H_{35}F_6P_3Ru$	$C_{40}H_{43}P_3F_6Ru$	$C_{44}H_{41}P_2F_3O_3S$ Ru	$C_{42}H_{38}P_2Ru$
Molecular mass	1845.460	458.325	954.760	795.160
Crystal system	triclinic	monoclinic	triclinic	monoclinic
Space group	$P\bar{1}$	Pn	$P\bar{1}$	$P2_1/n$
Lattice constants	a = 1283.9 (3) pm	a = 1004.7 (2) pm	a = 1006.0 (2) pm	a = 1088.3 (2) pm
	b = 1316.1 (3) pm	b = 1935.2 (4) pm	b = 1162.2 (2) pm	b = 1890.2 (4) pm
	c = 1398.8 (3) pm	c = 2056.3 (4) pm	c = 1847.1 (4) pm	c = 1795.5 (4) pm
	α = 82.55(3)°	α = 90.00(0)°	α = 75.13(3)°	α = 90.00(0)°
	β = 63.39(3)°	β = 90.66(3)°	β = 83.98(3)°	β = 95.55(3)°
	γ = 67.95(3)°	γ = 90.00(0)°	γ = 81.70(3)°	γ = 90.00(0)°
Cell volume	1957·10^6 pm^3	3998·10^6 pm^3	2060·10^6 pm^3	3676·10^6 pm^3
Molecular units per cell	Z = 2	Z = 4	Z = 2	Z = 4
Density (calculated)	1.566 g/cm^3	1.523 g/cm^3	1.539 g/cm^3	1.437 g/cm^3
Measuring device	Nonius Kappa CCD	Nonius Kappa CCD	Nonius Kappa CCD	Nonius Kappa CCD
Temperature	200 K	200 K	200 K	200 K
Number of reflections for cell refinement				
Scan range	3.8° < 2θ < 52.0°	4.5° < 2θ < 52.1°	3.7° < 2θ < 49.0°	3.1° < 2θ < 52.1°
Method	ω-scan, Δω = 1.0°	ω-scan, Δω = 1.0°	ω-scan, Δω = 1.0°	ω-scan, Δω = 1.0°
Scan speed	5 sec/frame	10 sec/frame	6 sec/frame	30 sec/frame
Measured reflections	31037	17579	32432	127717
Unique reflections	7645	11424	6865	7242
Observed reflections [$I \geq 2\sigma(I)$]	5789	8873	5503	5117
Number of parameters refined	484	872	519	446
Maximum of residual electron density	1.75 × 10^{-6} e/pm^3	0.88 × 10^{-6} e/pm^3	2.06 × 10^{-6} e/pm^3	0.97 × 10^{-6} e/pm^3
Agreement factors	R_1 = 0.049	R_1 = 0.044	R_1 = 0.044	R_1 = 0.047
(F^2 refinement)	R_w = 0.137	R_w = 0.102	R_w = 0.114	R_w = 0.126

[a] The crystals tend to contain solvate molecules. The number and type of solvate molecules found per formula unit is given in the column header.

(Figure 3). The secondary interaction within the *tripod*CpL_2Ru templates, which governs their conformation, will be closely similar in all of its *tripod*CpL_2RuL' compounds (L′ = coligand) due to the fact that the distances and valence angles within the templates are also closely similar. It can be seen from Figures 1 and 3 that the conformations adopted by the *tripod*CpL_2Ru templates are in fact rather similar for the whole group of compounds. This is shown in a quantitative way by the torsion angles C_o−C_i−P−Hc (where Hc denotes an auxiliary point fixed to

Table 8. Analytical data for compounds **1**−**3a**

	1	**2**	**3a**
IR: $\tilde{\nu}$ [$^{-1}$]	−	CO: 1966 vs; PF: 839 vs	CN: 2070 m
$^1H\{^{31}P\}$ NMR	CD_2Cl_2	CD_2Cl_2	$CDCl_3$
C**H**$_3$	1.53 s, 3 H	1.83 s, 3 H	1.58 s, 3 H
C**H**$_2$Cp	1.67 s, 2 H	2.22 s, 2 H	1.91 s, 2 H
C**H**$_2$P(H$_a$) [a]	2.15 d ($^2J_{HH}$ = 15 Hz), 2 H	2.39 d ($^2J_{HH}$ = 15.8 Hz), 2 H	2.07 d ($^2J_{HH}$ = 15.4 Hz), 2 H
C**H**$_2$P(H$_b$) [a]	2.47 d ($^2J_{HH}$ = 15 Hz), 2 H	2.78 d ($^2J_{HH}$ = 15.8 Hz), 2 H	2.44 d ($^2J_{HH}$ = 15.4 Hz), 2 H
Cp**H**$_\alpha$; Cp**H**$_\beta$	4.19 s, 2 H; 5.09 s, 2 H	4.75 s, 2 H; 5.70 s, 2 H	4.19 s, 2 H; 5.19 s, 2 H
arom. H	6.85−8.01 m, 20 H	7.07−7.58 m, 20 H	6.84−8.0 m, 20 H
R *isonitrile*	−	−	−
^{31}P NMR (PPh_2; PF_6)	34.98 s	45.3 s; −144.1, $^1J_{PF}$ = 713 Hz	44.61 s
$^{13}C\{^1H\}$ NMR [b]	CD_2Cl_2	CD_2Cl_2	$CDCl_3$
CH$_3$	34.1 t ($^3J_{CP}$ = 13 Hz)	33.9 m	34.6 t ($^3J_{CP}$ = 10 Hz)
CH$_3$**C**	49.3 m	51.1 br. s	50.6 m
CH$_2$Cp	37.3 s	36.7 s	38.5 s
CH$_2$P	35.1 ps. t ($^1J_{CP}$ = $^3J_{CP}$ = 20 Hz)	33.2 ps. t ($^1J_{CP}$ = $^3J_{CP}$ = 18 Hz)	35.0 ps. t ($^1J_{CP}$ = $^3J_{CP}$ = 18 Hz)
C$_i$*Cp*	68.7 s	88.7 s	81.1 s
C$_\beta$*Cp*; **C**$_\alpha$*Cp*	83.3 s; 94.1 s	84.9 s; 101.2 s	80.6 s; 96.3 s
C$^{m1/2}$H*arom.* [c]	127.8; 128.5 ps. t ($^3J_{CP}$ = $^5J_{CP}$ = 5 Hz)	129.4; 129.7, ps. t ($^3J_{CP}$ = $^5J_{CP}$ = 5 Hz)	128.1; 128.8 ps. t ($^3J_{CP}$ = $^5J_{CP}$ = 5 Hz)
C$^{o1/2}$H*arom.* [c]	131.6−132.0 m	130.5; 131.3 m	131.3−131.9 m
C$^{p1/2}$H*arom.* [c]	129.3 s	130.8 s	128.8 s; 129.5 s
C^{i1}*arom.*	138.8 ps. t ($^1J_{CP}$ = $^3J_{CP}$ = 15 Hz)	132.7 ps. t ($^1J_{CP}$ = $^3J_{CP}$ = 27 Hz)	136.9 ps. t ($^1J_{CP}$ = $^3J_{CP}$ = 19.5 Hz)
C^{i2}*arom.*	144.4 ps. t ($^1J_{CP}$ = $^3J_{CP}$ = 15 Hz)	139.3 t ($^1J_{CP}$ = $^3J_{CP}$ = 27.5 Hz)	143.4 ps. t ($^1J_{CP}$ = $^3J_{CP}$ = 23 Hz)
CN /**C**O	−	203.2 m	146.4
elemental analysis	C 63.80 *64.09*, H 5.20 *5.62*, P 9.67	C 54.06 *54.50*, H 4.28 *4.86*, P 11.95	C 66.66 *65.37*, H 5.27 *5.58*, N 2.22
calculated/*found*	*9.34*	*11.83*	*2.01*, P 9.82 *9.30*
mass spectrometry	EI: 640 [M$^+$]; 605 [M$^+$ − Cl]	FAB: 633 [M$^+$]; 605 [M$^+$ − CO]	EI: 631 [M$^+$]; 605 [M$^+$ − CN]

[a] Diastereotopic hydrogen atoms at CH_2P groups. − [b] CH_3, CH_2, CH, and C carbons were assigned by means of a 135° DEPT experiment. − [c] Individual assignment of the resonances to the different classes of phenyl rings was not possible.

the phosphorus atom with the resulting vector pointing in the direction C4−Ru towards the observer), which indicate that − with the exception of **5** − the phenyl rings tend to be aligned parallel to this auxiliary vector within a maximum deviation of 39° and with an average deviation of only 18° (Tables 5 and 6).

It is apparent from Figure 3 (**5**) that the η^2-coordinated 1,2-diphenylacetylene coligand interferes with the orientation of the phenyl groups of the template. The data in Table 5 reveals correspondingly large torsion angles up to a maximum value of 45°. Whereas constitutionally the templates *tripod*CpL_2Ru have mirror symmetry, conformationally this cannot be so due to the skew within the chelate scaffolding. The entries in Figures 1 and 3 and Tables 4−6 have been arranged such that the torsion of the scaffolding has the same sense in all the structures. It can be seen from Figure 3 as well as from Tables 5 and 6 that the most prominent torsion occurs with respect to the C4−C2−P2−Ru part of the scaffolding (−18 to −34°). The least prominent skew is consistently observed for the C4−C1−P1−Ru part (+1 to −9°), with the skew of the part bearing the cyclopentadienyl molecule, C4−C3−C6−Ru, being intermediate −5 to −16° (Figures 1 and 3; Tables 5 and 6). It appears that the difference in the torsion angles C4−C1−P1−Ru (small) and C4−C2−P2−Ru (large) is mirrored in the Ru−P distances, which, although similar, are systematically larger for Ru−P1 (mean 228.5 pm) than for Ru−P2 (mean 227.0 pm) in all the compounds studied (Table 4). This may be taken as an indication of some strain within the chelate cage, which is also evident from the Ru−C_{Cp} distances. The sequence of these distances is such that the bond to the carbon atom C6 (mean 220.3 pm), which is linked to the chelate cage, tends to be the shortest, while the bonds to C8/C9 are systematically longer (mean values 227.4 and 225.7 pm, respectively); the Ru−C7/C10 bonds have intermediate lengths (mean values 223.1 and 222 pm). This pattern of bond distances corresponds to a shift of the ruthenium atom parallel to the plane of the Cp ligand in the direction of C6, away from its ideal position below the centre of this ring (*d* in Table 4). The distances within the Cp ligand respond to this asymmetry in a systematic way. The C6−C7/C6−C10 bonds are longer (mean 143.3 pm) than the C7−C8/C9−C10 bonds (mean 140.7 pm), with the remaining C8−C9 bond also being rather long (mean 142.7 pm). This pattern is seen in all the individual compounds investigated and thus represents a general trend. In a few cases where at first glance this pattern appears to be contradicted by the numerical values, the standard deviations of these values make the apparent contradiction insignificant.

Taken together, the indications of strain within the chelate scaffolding are only minor since the variance in the geometrical parameters, which would be expected to have equal values in an unstrained system, is not significantly larger than that observed in compounds where there is no steric strain imposed by a chelate cage.[4,12,19] The chemical behaviour of the *tripod*CpL_2Ru template can thus be expected to be similar to that exhibited by the non-chelate templates of the type CpL_2Ru, as has indeed been observed.

Table 9. Analytical data for compounds **3b**−**4a**

	3b·OTf	**3c**·PF_6	**4a**·PF_6
IR: $\tilde{\nu}$ [$^{-1}$]	CN: 2127 s; OTf: 1265 s, 1152 m, 1030 m	CN: 2143 br, 836 vs	CN: 2266 vw; PF: 839 vs
$^1H\{^{31}P\}$ NMR	CD_2Cl_2	CD_2Cl_2	CD_2Cl_2
C**H**$_3$	1.73 s, 3 H	1.71 s, 3 H	1.62 s, 3 H
C**H**$_2$Cp	2.07 s, 2 H	2.08 s, 2 H	1.80 s, 2 H
C**H**$_2$P(H_a) [a]	2.25 d ($^2J_{HH}$ = 15.8 Hz), 2 H	2.26 d ($^2J_{HH}$ = 15.6 Hz), 2 H	2.20 d (J_{HH} = 15.6 Hz), 2 H
C**H**$_2$P(H_b) [a]	2.65 d ($^2J_{HH}$ = 15.8 Hz), 2 H	2.61 d ($^2J_{HH}$ = 15.6 Hz), 2 H	2.57 d (J_{HH} = 15.6 Hz), 2 H
Cp**H**$_\alpha$; Cp**H**$_\beta$	4.52 s, 2 H; 5.45 s, 2 H	4.52 s, 2 H; 5.39 s, 2 H	4.40 s, 2 H; 5.38 (+ solv.) s
arom. H	6.93−7.80 m, 20 H	6.86−7.62 m, 20 H	6.83−7.77 m, 20 H
R *isonitrile*	3.70 s, 3 H, CN*Me*	1.53, 1.88, 2.17, 4.15, 11H	2.56 s, 3 H, NC*Me*
^{31}P NMR (PPh_2; PF_6)	47.03 s	46.7 s; −144.2 $^1J_{PF}$ = 713 Hz	39.3 s; −144.1 $^1J_{PF}$ = 713 Hz
$^{13}C\{^1H\}$ NMR [b]	CD_2Cl_2	CD_2Cl_2	CD_2Cl_2
CH$_3$	34.0 m	34.2 m	33.9 t ($^3J_{CP}$ = 13 Hz)
CH$_3$**C**	50.9 t ($^2J_{CP}$ = 5 Hz)	51.0 m	49.8 t ($^2J_{CP}$ = 5 Hz)
CH$_2$Cp	37.3 s	37.6 s	36.5 s
CH$_2$P	34.1 ps. t ($^1J_{CP}$ = $^3J_{CP}$ = 20 Hz)	34.4 ps. t ($^1J_{CP}$ = $^3J_{CP}$ = 20 Hz)	34.4 ps. t ($^1J_{CP}$ = $^3J_{CP}$ = 19 Hz)
C$_i$*Cp*	84.2 s	84.4 s	72.5 s
C$_\beta$*Cp*; **C**$_\alpha$*Cp*	82.2 s; 98.5 s	82.4 s; 98.6 s	82.4 s; 95.9 s
C$^{m1/2}$H*arom.* [c]	128.7; 129.2 ps. t ($^3J_{CP}$ = $^5J_{CP}$ = 5 Hz)	128.6; 129.3 ps. t ($^3J_{CP}$ = $^5J_{CP}$ = 5 Hz)	128.6; 129.2 ps. t ($^3J_{CP}$ = $^5J_{CP}$ = 5 Hz)
C$^{o1/2}$H*arom.* [c]	130.5; 131.6 ps. t ($^2J_{CP}$ = $^4J_{CP}$ = 5 Hz)	130.9; 131.5 ps. t ($^2J_{CP}$ = $^4J_{CP}$ = 5 Hz)	130.6; 131.6 ps. t ($^2J_{CP}$ = $^4J_{CP}$ = 5 Hz)
C$^{p1/2}$H*arom.* [c]	129.9 s, 130.6 s	129.8; 130.6 s	129.6; 130.3 s
C^{i1}*arom.*	135.0 ps. t ($^1J_{CP}$ = $^3J_{CP}$ = 23 Hz)	135.3 ps. t ($^1J_{CP}$ = $^3J_{CP}$ = 23 Hz)	136.3 ps. t ($^1J_{CP}$ = $^3J_{CP}$ = 19 Hz)
C^{i2}*arom.*	141.1 ps. t ($^1J_{CP}$ = $^3J_{CP}$ = 25 Hz)	141.3 ps. t ($^1J_{CP}$ = $^3J_{CP}$ = 25 Hz)	141.8 ps. t ($^1J_{CP}$ = $^3J_{CP}$ = 19 Hz)
CN or N**C**	**C**F_3: 118.3 s; **C**N: 124.7	n. f.	127.7 s
CN**R** or NC**R**	31.0, CN***Me***	24.0, 25.5, 33.9 **C**H_2; 55.9 **C**H	4.8 NC**Me**
elemental analysis	C 55.92 *56.22*, H 4.57 *5.14*, N 1.76 *1.79*, P	C 57.34 *57.57*, H 5.16 *5.56*, N 1.63 *1.87*, P	C 54.69 *55.61*, H 4.59 *5.28*, N 1.77 *1.73*, P
calculated/*found*	7.79 *7.49*	10.82 *10.72*	11.75 *11.20*
mass spectrometry	FAB: 646 [M^+]; 605 [M^+ − CNMe]	FAB: 714 [M^+]; 605 [M^+ − CNCy]	FAB: 646 [M^+]; 604 [M^+ − NCMe]

[a] Diastereotopic hydrogen atoms at CH_2P groups. − [b] CH_3, CH_2, CH, and C carbons were assigned by means of a 135° DEPT experiment. − [c] Individual assignment of the resonances to the different classes of phenyl rings was not possible.

Conclusion

The chelate ligand $CH_3C(CH_2C_5H_4)(CH_2PPh_2)_2Li$ forms templates $CH_3C(CH_2\text{-}\eta^5\text{-}C_5H_4)(CH_2\text{-}\eta^1\text{-}PPh_2)_2Ru$, *tripod*$CpL_2Ru$, which bind to coligands L′ in a similar manner as known for the non-chelate analogues $CpRuL_2$. With anionic ligands (L′ = Cl^-, CN^-, acetylides), neutral compounds *tripod*CpL_2RuL' are obtained. With neutral ligands (L′ = nitriles, isonitriles, vinylidenes, allenylidenes) cationic species [*tripod*$CpL_2RuL']^+$ are formed. The reactivity of the template and its coordination compounds is similar to that reported for the non-chelate analogues $CpRuL_2$.[4][19]

Structural analyses of nine coordination compounds containing the *tripod*CpL_2Ru entity show that the conformation of the template is little affected by the nature of coligand bonded to it. The results also demonstrate that there is no great strain within the chelate cage. Nevertheless, the cage is rather rigid, such that inversion − which may be a problem in the reaction of non-chelate compounds of this type − cannot occur. Reactions of chiral versions of this template can thus be expected to allow for undisturbed diastereochemical control.

The barriers to rotation of the vinylidene fragments about their bonds to the *tripod*CpL_2Ru template amount to $\Delta H^{\neq}$ = 40.3 kJmol^{-1} in C=CMe(*t*Bu) and $\Delta H^{\neq}$ = 47.9 kJmol^{-1} in C=CMe(Ph), as estimated by means of ^{31}P-NMR spectroscopy. These values lie in a range typical for the rotation of such single-faced π-acceptors about their Ru−C bond in unstrained CpL_2Ru vinylidene compounds.

Experimental Section

General Remarks: Unless noted otherwise, all manipulations were carried out under argon by means of standard Schlenk techniques. All solvents were dried by standard methods[32] and distilled under argon. The solvents $CDCl_3$ and CD_2Cl_2 used for NMR spectroscopic measurements were degassed by three successive "freeze-pump-thaw" cycles and dried over 4 Å molecular sieves. − NMR: Bruker Avance DPX 200 at 200.12 MHz (^1H), 50.323 MHz ($^{13}C\{^1H\}$), 81.015 MHz ($^{31}P\{^1H\}$) or Bruker Avance DRX 500 at 500.13 MHz (^1H), 125.76 MHz ($^{13}C\{^1H\}$), 202.46 MHz ($^{31}P\{^1H\}$); at 303 K unless stated otherwise; chemical shifts (δ) in ppm with respect to residual solvent peaks as internal standards: $CDCl_3$ (^1H: δ = 7.27; ^{13}C: δ = 77.0); CD_2Cl_2 (^1H: δ = 5.32; ^{13}C: δ = 53.8). ^{31}P chemical shifts (δ) in ppm with respect to 85% H_3PO_4 (^{31}P: δ = 0) as external standard. − IR: Bruker IFS-66 spectrophotometer; KBr discs. − MS (EI): Finnigan MAT 8230: Fast-atom bombardment (FAB) with xenon; matrix: 4-nitrobenzyl alcohol. − HR-MS (EI): VG ZAB 2F and HR-MS (FAB) JEOL JMS 700; matrix: 4-nitrobenzyl alcohol. − Elemental analyses: Microanalytical Laboratory of the Organisch-Chemisches Institut, Universität Heidelberg. − Melting points: Gallenkamp MFB-595 010; values are not corrected. − Cyclic voltammetry: Metrohm "Universal Meß- und Titriergefäß", Metrohm GC electrode RDE 628, platinum electrode, SCE electrode, Princeton Applied Research potentiostat Model 273; substrate concentration 10^{-3} M in 0.1 M nBu$_4$NPF_6/CH_2Cl_2.

Crystallographic Structure Determinations: The measurements were carried out on a Siemens P4 four-circle diffractometer (for **3a**) or on an Enraf−Nonius Kappa CCD diffractometer, using graphite-monochromated Mo-K_α radiation throughout. In the case of the Siemens P4 four-circle diffractometer measurements, the intensities

Table 10. Analytical data for compounds **4b**−**6**

	4b·PF_6	**5**·PF_6	**6**·PF_6
IR: $\tilde{\nu}$ [$^{-1}$]	CN: 2218 s; PF: 843 vs	PF: 1905 vw; 838 vs	CC: 1919 br; PF: 838 vs
$^1H\{^{31}P\}$ NMR	CD_2Cl_2	CD_2Cl_2	CD_2Cl_2
C**H**$_3$	1.61 s, 3 H	1.17 s, 3 H	1.86 s, 3 H
C**H**$_2$Cp	1.81 s, 2 H	2.55 s, 2 H	2.39 s, 2 H
C**H**$_2$P(H$_a$) [a]	2.21 d (J_{HH} = 15.6 Hz), 2 H	2.34 d ($^2J_{HH}$ = 16 Hz), 2 H	2.40 d ($^2J_{HH}$ = 16 Hz), 2 H
C**H**$_2$P(H$_b$) [a]	2.63 d (J_{HH} = 15.6 Hz), 2 H	2.55 d ($^2J_{HH}$ = 16 Hz), 2 H	2.83 d ($^2J_{HH}$ = 16 Hz), 2 H
Cp**H**$_\alpha$; Cp**H**$_\beta$	4.45 s, 2 H; 5.47 s, 2 H	5.51 s, 2 H; 5.68 s, 2 H	4.79 s, 2 H; 5.86 s, 2 H
arom. H	6.85−7.78 m, 25 H	6.61−7.44 m, 30 H	7.79−8.00 m, 30 H
coligand	[d]	[d]	[d]
^{31}P NMR (PPh_2; PF_6)	39.5 s; −144.1 $^1J_{PF}$ = 713 Hz	38.80 s; −144.1 $^1J_{PF}$ = 713 Hz	50.4 s; −144.1 $^1J_{PF}$ = 713 Hz
$^{13}C\{^1H\}$ NMR [b]	CD_2Cl_2	CD_2Cl_2	CD_2Cl_2
CH$_3$	33.9 m	33.9 t ($^3J_{CP}$ = 13 Hz)	34.1 m
CH$_3$**C**	49.9 m	47.9 m	50.9 t ($^2J_{CP}$ = 3.7 Hz)
CH$_2$Cp	36.5 s	35.9 s	37.9 s
CH$_2$P	34.3 ps. t ($^1J_{CP}$ = $^3J_{CP}$ = 18.5 Hz)	39.0 ps. t ($^1J_{CP}$ = $^3J_{CP}$ = 17 Hz)	33.4 pt ($^1J_{CP}$ = $^3J_{CP}$ = 17 Hz)
C$_i$*Cp*	73.8 s	86.1 s	93.5 s
C$_\beta$*Cp*; **C**$_\alpha$*Cp*	82.9 s; 96.4 s	89.2 s; 95.3 s	91.3 s; 100.1 s
C$^{m1/2}$H*arom.* [c]	128.7; 129.2 ps. t ($^3J_{CP}$ = $^5J_{CP}$ = 5 Hz)	128.2; 128.8 ps. t ($^3J_{CP}$ = $^5J_{CP}$ = 5 Hz)	128.8; 129.4 ps. t ($^3J_{CP}$ = $^5J_{CP}$ = 5 Hz)
C$^{o1/2}$H*arom.* [c]	130.7; 131.6 ps. t ($^1J_{CP}$ = $^3J_{CP}$ = 5 Hz)	132.9; 133.4 ps. t ($^2J_{CP}$ = $^4J_{CP}$ = 5 Hz)	131.3 ps. t ($^2J_{CP}$ = $^4J_{CP}$ = 5 Hz)
C$^{p1/2}$H*arom.* [c]	129.8; 130.6 s	128.5, 129.1, 131.1, 130.7[d]	129.6, 130.4, 130.7, 130.9[d]
C^{i1}*arom.*	136.2 ps. t ($^1J_{CP}$ = $^3J_{CP}$ = 20 Hz)	134.4 ps. t ($^1J_{CP}$ = $^3J_{CP}$ = 25 Hz)	133.6 ps. t ($^1J_{CP}$ = $^3J_{CP}$ = 26 Hz)
C^{i2}*arom.*	141.5 ps. t ($^1J_{CP}$ = $^3J_{CP}$ = 25.5 Hz)	139.6 ps. t ($^1J_{CP}$ = $^3J_{CP}$ = 27 Hz)	140.1 ps. t ($^1J_{CP}$ = $^3J_{CP}$ = 27 Hz)
C$_\alpha$, **C**$_\beta$, **C**$_\gamma$	112.3 s, N**C**Ph	80.5 s, η^2-**CC**	291.9 m; 211.1, 152.0
coligand arom. **C**H	128.1 **C**^{i}; 130.2, 132.5, 134.1	132.0, **C**^{i}(**Ph**CC**Ph**)[d]	144.0, **C**^{i}Ph[d]
elemental analysis	C 57.75 *58.94*, H 4.49 *4.94*, N 1.64 *1.68*,	C 62.14 *60.82*, H 4.67 *4.98*, P 10.01 *n.b.*	C 62.92 *62.42*, H 4.61 *4.85*, P 9.89 *9.95*
calculated/*found*	P 10.90 *10.97*		
mass spectrometry	FAB: 708 [M$^+$]; 605 [M$^+$ − NCPh]	FAB: 783 [M$^+$]; 605 [M$^+$ − C_2Ph_2]	FAB: 796 [M$^+$]; 605 [M$^+$ − R]

[a] Diastereotopic hydrogen atoms at CH_2P groups. − [b] CH_3, CH_2, CH, and C carbons were assigned by means of a 135° DEPT experiment. − [c] Individual assignment of the resonances to the different classes of phenyl rings was not possible. − [d] Differentiation between the phenyl resonances of the coligand and the phenyl resonances of the tripodal ligand was not possible.

Table 11. Analytical data for compounds **7a**−**7c**

	7a·PF_6	**7b**·PF_6	**7c**·PF_6
IR: $\tilde{\nu}$ [$^{-1}$]	CC: 1624 m; PF: 840 vs	CC: 1638 m; PF: 840 vs	CC: 1641 m; PF: 840 vs
$^1H\{^{31}P\}$ NMR	CD_2Cl_2	CD_2Cl_2	CD_2Cl_2
C**H**$_3$	1.81 s, 3 H	1.73 s, 3 H	1.84 s, 3 H
C**H**$_2$Cp	2.22 s, 2 H	2.17 s, 2 H	2.31 s, 2 H
C**H**$_2$P(H$_a$) [a]	2.37 d ($^2J_{HH}$ = 16 Hz), 2 H	2.36 d ($^2J_{HH}$ = 15.8 Hz), 2 H	2.40 d ($^2J_{HH}$ = 16 Hz), 2 H
C**H**$_2$P(H$_b$) [a]	2.82 d ($^2J_{HH}$ = 16 Hz), 2 H	2.75 d ($^2J_{HH}$ = 15.8 Hz), 2 H	2.83, d ($^2J_{HH}$ = 16 Hz), 2 H
Cp**H**$_\alpha$; Cp**H**$_\beta$	4.75 s, 2 H; 5.88 s, 2 H	4.72 s, 2 H; 5.72 s, 2 H	4.89 s 2 H; 5.99 s, 2 H
arom. H	6.93−7.47 m, 20 H	6.81−7.65 m, 20 H	6.51−7.51 m, 25 H
=C**H**(R)	4.65 t ($^4J_{HP}$ = 4 Hz), 2 H	4.91 t ($^4J_{HP}$ = 4 Hz), 1 H	6.2 t ($^4J_{HP}$ = 3.4 Hz), 1 H
=C**R**(H)	−	1.31 s, 9 H	[d]
^{31}P NMR (PPh_2; PF_6)	48.8 s; −144.1 $^1J_{PF}$ = 713 Hz	48.9 s; −144.1 $^1J_{PF}$ = 713 Hz	48.8 s; −144.1 $^1J_{PF}$ = 713 Hz
$^{13}C\{^1H\}$ NMR [b]	CD_2Cl_2	CD_2Cl_2 (500 MHz)	CD_2Cl_2
CH$_3$	33.9 m	33.9 t ($^3J_{CP}$ = 13 Hz)	33.6 m
CH$_3$**C**	50.8 m	50.5 br. s	50. 6 t ($^2J_{CP}$ = 3.6 Hz)
CH$_2$Cp	37.5 s	37.4	37.3
CH$_2$P	33.4 ps. t ($^1J_{CP}$ = $^3J_{CP}$ = 15 Hz)	34.5 ps. t ($^1J_{CP}$ = $^3J_{CP}$ = 20 Hz)	33.8 ps. t ($^1J_{CP}$ = $^3J_{CP}$ = 17 Hz)
C$_i$*Cp*	92.8 s	92.2	93.1
C$_\beta$*Cp*; **C**$_\alpha$*Cp*	90.8 s; 101.3 s	90.7 s; 100.9 s	91.3 s; 101.5 s
C$^{m1/2}$H*arom.*[c]	128.8; 129.5 ps. t ($^3J_{CP}$ = $^5J_{CP}$ = 5 Hz)	128.6; 129.4 ps. t ($^3J_{CP}$ = $^5J_{CP}$ = 5 Hz)	128.8; 129.5 ps. t ($^3J_{CP}$ = $^5J_{CP}$ = 5 Hz)
C$^{o1/2}$H*arom.* [c]	131.3 m	131.6 m	131.5 m
C$^{p1/2}$H*arom.* [c]	130.6 s	130.6; 131.1 s	130.7; 131.3 s
C^{i1}*arom.*	132.2 ps. t ($^1J_{CP}$ = $^3J_{CP}$ = 27.5 Hz)	133.0 ps. t ($^1J_{CP}$ = $^3J_{CP}$ = 25 Hz)	134.2 ps. t ($^1J_{CP}$ = $^3J_{CP}$ = 20 Hz)
C^{i2}*arom.*	139.4 ps. t ($^1J_{CP}$ = $^3J_{CP}$ = 27.5 Hz)	139.6 ps. t ($^1J_{CP}$ = $^3J_{CP}$ = 25 Hz)	139.7 ps. t ($^1J_{CP}$ = $^3J_{CP}$ = 25 Hz)
C$_\alpha$; **C**$_\beta$	346.5 m; 98.7 s	348.8 m; 126.7 s	353.8 m; 119.3 s
=C**R**(H)	−	32.4 *t*Bu; 32.3 C$_q$*t*Bu	126.8, 127.0 s, 129.4 **C**H*Ph*
elemental analysis	C 55.75 *55.75*, H 4.55 *4.83*, P 11.98 *11.96*	C 57.76 *58.38*, H 5.21 *5.24*, P 11.17 *10.68*	C 59.23 *59.99*, H 4.26 *4.82*, P 10.91 *10.92*
calculated/*found*			
mass spectrometry	FAB: 631 [M$^+$]; 605 [M$^+$ − R]	FAB: 687 [M$^+$]; 605 [M$^+$ − R]	FAB: 707 [M$^+$]; 605 [M$^+$ − R]

[a] Diastereotopic hydrogen atoms at CH_2P groups. − [b] CH_3, CH_2, CH, and C carbons were assigned by means of a 135° DEPT experiment. − [c] Individual assignment of the resonances to the different classes of phenyl rings was not possible.

Table 12. Analytical data for compounds **7d**−**8**

	7d·OTf	**7e**·OTf	**8**·PF_6
IR: $\tilde{\nu}$ [$^{-1}$]	CC: 1649 br; OTf: 1264 s, 1147, 1030	CC: 1647 br; OTf: 1265 s, 1147, 1030	CO: 1246 m; PF: 840 vs
$^1H\{^{31}P\}$ NMR	CD_2Cl_2	CD_2Cl_2	CD_2Cl_2
C**H**$_3$	1.75 s, 3 H	1.84 s, 3 H	1.67 s, 3 H
C**H**$_2$Cp	2.24 s, 2 H	2.32 s, 2 H	2.06 s, 2 H
C**H**$_2$P(H_a) [a]	2.28 d ($^2J_{HH}$ = 16 Hz), 2 H	2.37 d ($^2J_{HH}$ = 16 Hz), 2 H	2.22 d ($^2J_{HH}$ = 16 Hz), 2 H
C**H**$_2$P(H_b) [a]	2.74 d ($^2J_{HH}$ = 16 Hz), 2 H	2.81 d ($^2J_{HH}$ = 16 Hz), 2 H	2.71 d ($^2J_{HH}$ = 16 Hz), 2 H
Cp**H**$_\alpha$; Cp**H**$_\beta$	4.93 s, 2 H; 5.84 s, 2 H	4.92 s, 2 H; 6.03 s, 2 H	4.74 s; 5.56 s
arom. H	6.95−7.45 m; 20 H	6.83−7.45 m, 25 H	6.7−7.9 m, 20 H
=CC**H**$_3$(R)	2.09 s, 3 H	2.52 s, 3 H [d]	3.31 s *Me*, 3 H; 3.95 s *OMe*, 3 H
=C(Me)**R**	1.32 s, 9 H, *t*Bu		
^{31}P NMR (PPh_2; PF_6)	48.7 s	49.3 s	47.8 s; −144.1 $^1J_{PF}$ = 713 Hz
$^{13}C\{^1H\}$ NMR [b]	CD_2Cl_2	CD_2Cl_2	CD_2Cl_2
CH$_3$	33.9 t ($^3J_{CP}$ = 13 Hz)	33.8 m	34.2 t ($^3J_{CP}$ = 13 Hz)
CH$_3$**C**	50.0 br. s	50.4 m	50.1 br. s
CH$_2$Cp	37.3 s	37.2 s	38.6 s
CH$_2$P	35.9 ps. t ($^1J_{CP}$ = $^3J_{CP}$ = 17 Hz)	34.2 ps. t ($^1J_{CP}$ = $^3J_{CP}$ = 17 Hz)	35.8 ps. t ($^1J_{CP}$ = $^3J_{CP}$ = 17 Hz)
C$_i$*Cp*	91.6	92.9	87.4 s
C$_\beta$*Cp*; **C**$_\alpha$*Cp*	90.3 s; 100.5 s	90.8 s; 101.2 s	88.2 s; 100.8 s
C$^{m1/2}$H*arom.* [c]	128.7; 129.2 ps. t ($^3J_{CP}$ = $^5J_{CP}$ = 5 Hz)	128.8; 129.3 ps. t ($^3J_{CP}$ = $^5J_{CP}$ = 5 Hz)	127.9; 129.0 ps. t ($^3J_{CP}$ = $^5J_{CP}$ = 5 Hz)
C$^{o1/2}$H*arom.* [c]	131.9; 132.2 ps. t ($^2J_{CP}$ = $^4J_{CP}$ = 5 Hz)	131.5; 131.8 ps. t ($^2J_{CP}$ = $^4J_{CP}$ = 5 Hz)	131.8; 132.1 ps. t ($^1J_{CP}$ = $^3J_{CP}$ = 5 Hz)
C$^{p1/2}$H*arom.* [c]	130.7; 131.2 s	130.6; 131.2 s	129.6; 130.6 s
C^{i1}*arom.*	133.8 ps. t ($^1J_{CP}$ = $^3J_{CP}$ = 27 Hz)	133.1 ps. t ($^1J_{CP}$ = $^3J_{CP}$ = 30 Hz)	134.5 ps. t ($^1J_{CP}$ = $^3J_{CP}$ = 23 Hz)
C^{i2}*arom.*	139.8 ps. t ($^1J_{CP}$ = $^3J_{CP}$ = 27.5 Hz)	139.5 ps. t ($^1J_{CP}$ = $^3J_{CP}$ = 27.5 Hz)	141.5 ps. t ($^1J_{CP}$ = $^3J_{CP}$ = 25.5 Hz)
=**C**$_\alpha$; =**C**$_\beta$	352.1 m; n.f.	353.8 m; n.f.	308.2 m
=C**C**H$_3$(R); =C**R**(Me)	9.5 Me; 30.5 *t*Bu; 32.7 C^q	12.3 *Me*; 125.0 C^i*Ph*; 127.2, 127.5 **C**H	59.8 *O***C**H$_3$; 47.6 **C**H$_3$
elemental analysis calculated/*found*	C 59.36 *59.16*, H 5.34 *5.44*, P 7.29 *7.82*	C 60.75 *61.21*, H 4.75 *5.32*, P 7.12 *7.85*	C 55.02 *56.16*, H 4.87 *5.21*, P 11.50 *11.10*
mass spectrometry	FAB: 701 [M$^+$]; 605 [M$^+$ − R]	FAB: 721 [M$^+$]; 605 [M$^+$ − R]	FAB: 664 [M$^+$]; 605 [M$^+$ − R]

[a] Diastereotopic hydrogen atoms at CH_2P groups. − [b] CH_3, CH_2, CH, and C carbons were assigned by means of a 135° DEPT experiment. − [c] Individual assignment of the resonances to the different classes of phenyl rings was not possible.

Table 13. Analytical data for compound **9**

	9a	**9b**
IR: $\tilde{\nu}$ [$^{-1}$]	CC: 2071 m	CC: 2056 m
$^1H\{^{31}P\}$ NMR	CD_2Cl_2	CD_2Cl_2
C**H**$_3$	1.57 s, 3 H	1.54 t ($^4J_{HP}$ = 3 Hz), 3 H
C**H**$_2$Cp	1.94 s, 2 H	1.91 s, 2 H
C**H**$_2$P(H_a) [a]	2.08 d ($^2J_{HH}$ = 15.4 Hz), 2 H	2.11 d ($^2J_{HH}$ = 15.4 Hz), 2 H
C**H**$_2$P(H_b) [a]	2.37 d ($^2J_{HH}$ = 15.4 Hz), 2 H	2.46 d ($^2J_{HH}$ = 15.4 Hz), 2 H
Cp**H**$_\alpha$; Cp**H**$_\beta$	4.15 s, 2 H; 4.95 s, 2 H	4.20 s, 2 H; 5.10 s, 2 H
arom. H	6.84−7.88 m, 20 H	6.8−7.88 m, 25 H
C≡C**R**	1.38 s, 9 H	*cf.* arom. H
^{31}P NMR (PPh_2)	45.1 s	45.6 s
$^{13}C\{^1H\}$ NMR [b]	CD_2Cl_2	CD_2Cl_2
CH$_3$	34.2 m	34.2 t ($^3J_{CP}$ = 12.4 Hz)
CH$_3$**C**	50.3 m	50.5 t ($^2J_{CP}$ = 5.5 Hz)
CH$_2$Cp	38.8 s	38.8 s
CH$_2$P	35.3 ps. t ($^1J_{CP}$ = $^3J_{CP}$ = 20 Hz)	35.1 ps. t ($^1J_{CP}$ = $^3J_{CP}$ = 18 Hz)
C$_i$*Cp*	80.8 s	81.7 s
C$_\beta$*Cp*; **C**$_\alpha$*Cp*	80.2 s; 95.7 s	80.5 s; 96.0 s
C$^{m1/2}$H*arom.* [c]	127.3; 128.2 ps. t ($^3J_{CP}$ = $^5J_{CP}$ = 5 Hz)	127.7; 128.4 ps. t ($^3J_{CP}$ = $^5J_{CP}$ = 5 Hz)
C$^{o1/2}$H*arom.* [c]	131.7; 132.2 ps. t ($^2J_{CP}$ = $^4J_{CP}$ = 5 Hz)	131.7; 131.8 ps. t ($^2J_{CP}$ = $^4J_{CP}$ = 5 Hz)
C$^{p1/2}$H*arom.* [c]	128.3; 128.9 s	122.8, 129.1, 130.7 [d]
C^{i1}*arom.*	138.9 ps. t ($^1J_{CP}$ = $^3J_{CP}$ = 17 Hz)	138.3 ps. t ($^1J_{CP}$ = $^3J_{CP}$ = 18 Hz)
C^{i2}*arom.*	145.3 ps. t ($^1J_{CP}$ = $^3J_{CP}$ = 21 Hz)	144.6 ps. t ($^1J_{CP}$ = $^3J_{CP}$ = 22 Hz)
C$_\alpha$≡; ≡**C**$_\beta$	92.2 m; 117.4 s	134.2 m; 112.2 s [d]
C≡C**R**	33.8 *t*Bu; 32.4 **C**$_q$*t*Bu	
elemental analysis calculated/*found*	C 70.06 *68.60*, H 6.17 *6.63*, P 9.03 *9.02*	C 71.48 *70.05*, H 5.43 *5.99*, P 8.78 *8.11*
mass spectrometry	EI: 687 [M$^+$]; 672 [M$^+$ − Me]	EI: 706 [M$^+$]; 604 [M$^+$ − C_2Ph]

[a] Diastereotopic hydrogen atoms at CH_2P groups. − [b] CH_3, CH_2, CH, and C carbons were assigned by means of a 135° DEPT experiment. − [c] Individual assignment of the resonances to the different classes of phenyl rings was not possible. − [d] Differentiation between the phenyl resonances of the coligand and the phenyl resonances of the tripodal ligand was not possible.

Table 14. Synthesis of complexes **3**−**9**

compound	coligand/procedure	reaction time/temp.	colour	yield [%]	m.p. [°C][a]	HR-MS (*m/z*) calcd.; *found*	crystallization method[d]
3b	MeO_3SCF_3 (0.07 mL, 0.7 mmol)/D	15 min/25°C	pale yellow	80	213 (dec.)	646.1366; *646.1407*[b]	–
3c	cyclohexyl isocyanide (0.08 mL, 0.8 mmol)/A	1 h/25°C	light yellow	95	230 (dec.)	–	–
4a	acetonitrile (7 mL)/A	6 h/25°C	yellow	88	188 (dec.)	646.1366; *646.1353*[b] 605.1101; *605.1149*	–
4b	benzonitrile (0.2 mL)/A	4 h/25°C	yellow	90	193 (dec.)	708.1523; *708.1624*[b] 707.1626; *707.1635*	I
5	1,2-diphenylacetylene (270 mg, 1.5 mmol)/B	18 h/25°C	yellow	92	180 (dec.)	783.1884; *783.1827*[b]	Ia
6	1,1-diphenyl-2-propynol (350 mg, 1.7 mmol)/A	18 h /25°C	purple	70−80[e]	187 (dec.)	–	II
7a	trimethylsilylacetylene (0.36 mL, 2.4 mmol)/B	18 h/25°C	yellow	90	210 (dec.)	–	III
7b	3,3-dimethyl-1-butyne/A (0.19 mL, 1.5 mmol)/A	15 min/reflux	yellow-brown	72	213 (dec.)	687.1884; *687.1899*[b] 605.1101; *605.1187*	III
7c	phenylacetylene (0.1 mL, 0.9 mmol)/A	15 min/reflux	red-brown	86	209 (dec.)	707.1571; *707.1579* [b] 605.1101; *605.1137*	–
7d	MeO_3SCF_3 (0.05 mL, 0.5 mmol)/D	20 min/25°C	orange-red	70	232	–	–
7e	MeO_3SCF_3 (0.05 mL, 0.5 mmol)/D	20 min /25°C	brick red	86	155	721.1727; *721.1722*[b] 605.1101; *605.1115*	I
8	trimethylsilylacetylene (0.23 mL, 1.5 mmol)/A	18 h /25°C	yellow-brown	95	198 (dec.)	663.1520; *663.1584*[b] 605.1101; *605.1178*	–
9a	NaOMe (10 mL)/C	1 h/25°C	yellow	75	190	686.1805; *686.1779*[c] 671.1571; *671.1577*	–
9b	NaOMe (10 mL)/C	1 h/25°C	yellow	71	155	706.1492; *706.1531*[c]	III

[a] dec. = decomposition. – [b] HR-FAB. – [c] HR-EI. – [d] I: vapour diffusion of diethyl ether into a CH_2Cl_2 solution of the complex, 25°C. Ia: slow diffusion of diethyl ether into a DCE solution of the complex, 25°C. II: slow evaporation of the solvent from a $CDCl_3$ solution of the complex. III: a saturated CH_2Cl_2 solution of the complex (at 25°C) was crystallized at −20°C. – [e] As found in 4 different experiments.

of three check reflections (measured every 100 reflections) remained constant throughout the data collection, thus indicating crystal and electronic stability. The data collected on the Siemens P4 diffractometer were corrected as usual, including an experimental absorption correction. The data from the Enraf−Nonius Kappa CCD device were processed using the standard Nonius software.[33] All calculations were performed using the SHELXT PLUS software package. Structures were solved by direct methods with the SHELXS-97 program and refined with the SHELXL-97 program.[34] Graphical handling of the structural data during solution and refinement was performed with XPMA.[35] Atomic coordinates and anisotropic thermal parameters of the non-hydrogen atoms were refined by full-matrix least-squares calculations. Data relating to the structure determinations are collected in Table 7. Crystallographic data (excluding structure factors) for the structures reported in this paper have been deposited with the Cambridge Crystallographic Data Centre as supplementary publication nos. CCDC-127499 to CCDC-127507. Copies of the data can be obtained free of charge on application to the CCDC, 12 Union Road, Cambridge CB2 1EZ, U.K. [Fax: (internat.) +44 (0)1223/336033; E-mail: deposit@ccdc.cam.ac.uk].

Preparation of *tripod*CpL_2RuCl (1): $CH_3C(CH_2C_5H_4)(CH_2PPh_2)_2Li$ (613 mg, 1.2 mmol) was added to a solution of $RuCl_2(PPh_3)_3$[11] (959 mg, 1.0 mmol) in 1,2-dichloroethane[36] (20 mL). After heating for 3 h at 90°C, the solvent was evaporated in vacuo and the orange-brown residue was purified by chromatography on Al_2O_3 (Brockmann activity grade III). Elution with 500 mL of diethyl ether removed the PPh_3. Using a 1:1 mixture of CH_2Cl_2/diethyl ether, the product was then eluted in an orange fraction. Chromatography on SiO_2 using diethyl ether/CH_2Cl_2, 10:1, as eluent also afforded **1**, but it was not possible to remove traces of non-reacted $RuCl_2(PPh_3)_3$ and PPh_3 (produced during the reaction) by this method. The purity of the $RuCl_2(PPh_3)_3$ was seen to play an important role in determining the yields; 40−60% of **1** could be obtained as an orange powder, which was found to decompose at 228°C. For all other analytical data, see Table 8. From a CH_2Cl_2 solution of **1** saturated at 30°C, orange crystals could be collected after 8 weeks at 25°C.

Preparation of *tripod*CpL_2RuCO^+ (2): $TlPF_6$ (89 mg, 0.26 mmol) was added to a solution of **1** (144 mg, 0.23 mmol) in 10 mL of CH_2Cl_2. The solution was completely degassed by performing several freeze-pump-thaw cycles and was then saturated with CO. After 18 h, the mixture had become yellow, TlCl was filtered off, and the solvent was removed in vacuo. The residual yellow solid was washed with diethyl ether (3 × 20 mL) and dried in vacuo to give **2** (96%) as a yellow powder (decomposing at 248°C). For analytical data, see Table 8. – HR-FAB: calcd. 633.1050; found 633.1072.

Preparation of *tripod*CpL_2RuCN (3a): KCN (20 mg, 0.31 mmol) was added to a solution of **1** (150 mg, 0.23 mmol) in 10 mL of CH_3OH. After refluxing for 15 min, the solution became lemon-yellow. The solvent was then removed and the residue was filtered through a plug of SiO_2 (∅: 2 cm, *l*: 5 cm) using < 300 mL of ethanol. Removal of the solvent from the filtrate afforded **3a** (81%) as a lemon-yellow powder, which was found to decompose above 242°C. Crystals suitable for X-ray analysis were obtained by solvent diffusion from a saturated $CDCl_3$ solution of **3a** at 25°C. For analytical data, see Table 8. – HR-EI: calcd. 631.1132; found 631.1170.

A: General Procedure for the Synthesis of [*tripod*$CpL_2RuL']^+$ Complexes (L′ = nitrile, isonitrile, allenylidene, vinylidene, and carbene;

3c, 4a, 4b, 6, 7b, 7c, and 8): To methanol (20 mL) were added *tripod*CpL_2RuCl **1** (190 mg, 0.3 mmol) and NH_4PF_6 (100 mg, 0.61 mmol) to give an orange suspension. An excess of the appropriate nitrile, isonitrile, or alkyne (Table 14) was then added to the solution, which was subsequently stirred for up to 18 h at 25°C or for up to 1 h under reflux. When the reaction was complete, the reaction mixture had changed colour − yellow in the case of nitriles and isonitriles, red-brown or purple with alkynes. The solvent was then evaporated in vacuo and the residue was redissolved in CH_2Cl_2. The resulting solution was filtered to remove NH_4Cl and the excess NH_4PF_6. The solvent was then evaporated once more and the residual solid was washed with diethyl ether (3 × 10 mL) to give the PF_6 salt of [*tripod*CpL_2RuL']$^+$ in analytically pure form. For analytical data, see Tables 9 to 12.

B: General Procedure for the Synthesis of [*tripod*CpL_2RuL']$^+$ Complexes (L′ = vinylidene, η²-alkynyl; 7a, 5): To a suspension of *tripod*CpL_2RuCl **1** (190 mg, 0.3 mmol) and $TlPF_6$ (115 mg, 0.31 mmol) in CH_2Cl_2 (15 mL) was added a fivefold excess of the appropriate alkyne (Table 14). Upon stirring at 25 °C for 18 h, the initially orange solution became yellow. The reaction mixture was then filtered, the filtrate was concentrated in vacuo, and the residue was washed with diethyl ether (3 × 10 mL) to give the PF_6 salts of the corresponding [*tripod*CpL_2RuL']$^+$ complexes in analytically pure form. For analytical data, see Tables 10, 11, and 14.

C: General Procedure for Transformation of Vinylidene Compounds (7) into Alkynyl Compounds (9): To a solution of 0.25 mmol of the appropriate vinylidene compound in 10 mL of methanol, sodium methoxide solution (prepared by treating 5 mg of Na with 10 mL of methanol) was added dropwise over a period of 1 min. The solution immediately turned yellow. After stirring for 1 h at 25°C, the solvent was removed in vacuo. The residue was redissolved in CH_2Cl_2, the resulting solution was filtered, and the solvent was removed once more. The product was extracted with diethyl ether (3 × 10 mL) and was in each case obtained as a lemon-yellow waxy powder (Table 14). For analytical data, see Tables 13 and 14.

D: General Procedure for Alkylations: To a solution of 0.3 mmol of **3a** or **9** in 10 mL of CH_2Cl_2 was added 0.05 mL of $F_3CSO_3CH_3$. After stirring for 15−30 min at 25 °C, the resulting mixture became almost colourless in the case of **3a** and red in the case of **9**. After filtration, the filtrate was concentrated in vacuo and the residue was washed with diethyl ether (3 × 10 mL). For analytical data, see Tables 9, 12, and 14.

Acknowledgments

This work was supported by the German Science Foundation (SFB 247) and the Fonds der Chemischen Industrie. A generous loan of ruthenium(III) chloride from Degussa AG, Frankfurt, is gratefully acknowledged. We are indebted to Dr. J. Groß and Mr. T. Jannack for performing mass spectrometric measurements, to Mr. D. Günauer for carrying out cyclovoltammetric experiments, and to the staff of the microanalytical laboratory of the Organisch-Chemisches Institut der Universität Heidelberg for providing elemental analyses.

[1] [1a] See for example: H. Brunner, *Top. Curr. Chem.* **1975**, *56*, 67−90. − [1b] H. Brunner, *Acc. Chem. Res.* **1979**, *12*, 250−257. − [1c] W. E. Watts, in: *Comprehensive Organomet. Chem.* **1982**, *Vol. 8*, 1013−1071 and references therein. − [1d] J. M. O′Connor, C. P. Casey, *Chem. Rev.* **1987**, *87*, 307−318.

[2] [2a] A. R. Cutler, K. Hanna, J. C. Vites, *Chem. Rev.* **1988**, *88*, 1363−1403. − [2b] M. Brookhart, W. B. Studabaker, *Chem. Rev.* **1987**, *87*, 411−432. − [2c] S. G. Davies, I. M. Dordor-Hedgecock, P. J. C. Easton, S. C. Preston, K. H. Sutton, J. C. Walker, *Bull. Soc. Chim. Fr.* **1987**, *124*, 608−630.

[3] H. Brunner, *Adv. Organomet. Chem.* **1980**, *18*, 151−206.

[4] S. G. Davies, J. P. McNally, A. J. Smallridge, *Adv. Organomet. Chem.* **1990**, *30*, 1−76.

[5] This problem has been analysed by quantum chemical modelling: T. Ward, O. Schafer, C. Daul, P. Hofmann, *Organometallics* **1997**, *16*, 3207−3215. It is found experimentally that compounds with 3d metals are less rigid than those containing 4d metals; cf. ref.[28a]

[6] [6a] H. Brunner, *Angew. Chem.* **1969**, *81*, 395; *Angew. Chem. Int. Ed. Engl.* **1969**, *8*, 382. − [6b] H. Brunner, *Angew. Chem.* **1971**, *83*, 274−285; *Angew. Chem. Int. Ed. Engl.* **1971**, *10*, 249. − [6c] H. Brunner, J. Aclasis, M. Langer, W. Steger, *Angew. Chem.* **1974**, *86*, 864−865; *Angew. Chem. Int. Ed. Engl.* **1974**, *13*, 810. − [6d] H. Brunner, K. Fisch, P. G. Jones, J. Salbeck, *Angew. Chem.* **1989**, *101*, 1558−1559; *Angew. Chem. Int. Ed. Engl.* **1989**, *28*, 1521.

[7] [7a] B. Antelmann, U. Winterhalter, G. Huttner, B. C. Janssen, J. Vogelgesang, *J. Organomet. Chem.* **1997**, *545−546*, 407−420. − [7b] B. Antelmann, G. Huttner U. Winterhalter, *J. Organomet. Chem.* **1998**, *553*, 433−441.

[8] [8a] B. Antelmann, G. Huttner, J. Vogelgesang, O. Walter, U. Winterhalter, *J. Organomet. Chem.* **1997**, *549*, 139−148. − [8b] B. Antelmann, G. Huttner U. Winterhalter, *J. Organomet. Chem.* **1998**, *555*, 119−125. − [8c] J. Vogelgesang, Diplomarbeit, **1996**, Heidelberg.

[9] M. I. Bruce, C. Hameister, A. G. Swincer, R. C. Wallis, *Inorg. Synth.* **1982**, *21*, 78−80.

[10] I. P. Evans, A. Spencer, G. Wilkinson, *J. Chem. Soc., Dalton Trans.* **1973**, 204−209.

[11] P. S. Hallmann, T. A. Stephenson, G. Wilkinson, *Inorg. Synth.* **1970**, *12*, 238−240.

[12] F. Morandini, G. Consiglio, B. Straub, G. Ciani, A. Sironi, *J. Chem. Soc., Dalton Trans.* **1983**, 2293−2298.

[13] Structure: [13a] M. I. Bruce, F. S. Wong, B. W. Skelton, A. H. White, *J. Chem. Soc., Dalton Trans.* **1981**, 1398−1405. − Reactivity: [13b] P. M. Treichel, D. A. Komar, P. J. Vincenti, *Inorg. Chim. Acta* **1984**, *88*, 151−152. − [13c] P. M. Treichel, P. J. Vincenti, *Inorg. Chem.* **1985**, *24*, 228−230. − [13d] H. E. Bryndza, P. J. Domaille, R. A. Paciello, J. E. Bercaw, *Organometallics* **1989**, *8*, 379−385.

[14] T. Blackmore, M. I. Bruce, F. G. A. Stone, *J. Chem. Soc., A* **1971**, 2376−2382.

[15] M. I. Bruce, R. C. Wallis, *Aust. J. Chem.* **1981**, *34*, 209−213.

[16] G. S. Ashby, M. I. Bruce, I. B. Tomkins, R. C. Wallis, *Aust. J. Chem.* **1979**, *32*, 1003−1016.

[17] B. E. R. Schilling, R. Hoffmann, D. L. Lichtenberger, *J. Am. Chem. Soc.* **1979**, *101*, 585−591.

[18] [18a] N. G. Bokiy, Yu. V. Gatilov, Yu. T. Struchkov, N. A. Ustynyuk, *J. Organomet. Chem.* **1973**, *54*, 213−219. − [18b] R. G. Ball, M. R. Burke, J. Takats, *Organometallics* **1987**, *6*, 1918−1924. − [18c] J. R. Lomprey, J. P. Selegue, *J. Am. Chem. Soc.* **1992**, *114*, 5518−5523.

[19] [19a] M. I. Bruce, A. G. Swincer, *Adv. Organomet. Chem.* **1983**, *22*, 59−127. − [19b] M. I. Bruce, *Chem. Rev.* **1991**, *91*, 197−257.

[20] J. Silvestre, R. Hoffmann, *Helv. Chim. Acta* **1985**, *68*, 1461−1506.

[21] Y. Wakatsuki, N. Koga, H. Yamazaki, K. Morokuma, *J. Am. Chem. Soc.* **1994**, *116*, 8105−8111.

[22] I. de los Ríos, M. J. Tenorio, M. C. Puerta, P. Valerga, *J. Am. Chem. Soc.* **1997**, *119*, 6529−6538.

[23] Y. Wakatsuki, N. Koga, H. Werner, K. Morokuma, *J. Am. Chem. Soc.* **1997**, *119*, 360−366.

[24] [24a] H. Werner, *Angew. Chem.* **1990**, *102*, 1109−1212, *Angew. Chem. Int. Ed. Engl.* **1990**, *29*, 1077. − [24b] H. Werner, *Nachr. Chem. Tech. Lab.* **1992**, *40*, 435−444. H. Werner, *J. Organomet. Chem.* **1994**, *475*, 45−55. − [24c] A. Höhn, H. Otto, M. Dziallas, H. Werner *J. Chem. Soc., Chem. Commun.* **1987**, 852−854. − [24d] A. Höhn, H. Werner, *J. Organomet. Chem.* **1990**, *382*, 255. − [24e] F. J. Garcia Alonso, A. Höhn, J. Wolf, H. Otto, H. Werner, *Angew. Chem.* **1985**, *97*, 401−402, *Angew. Chem. Int. Ed. Engl.* **1985**, *24*, 406.

[25] [25a] J. P. Selegue, *Organometallics* **1982**, *1*, 217−218. − [25b] H. Le Bozec, K. Ouzzine, P. H. Dixneuf, *J. Chem. Soc., Chem. Commun.* **1989**, 219−221.

[26] N. M. Kostic, R. F. Fenske, *Organometallics* **1982**, *1*, 974−982.

[27] [27a] G. Consiglio, F. Bangeter, C. Darpin, *Organometallics* **1984**,

3, 1446−1448. − [27b] M. P. Gamasa, J. Gimeno, E. Lastra, B. M. Martin, *Organometallics* **1992**, *11*, 1373−1381.
[28] [28a] G. Consiglio, F. Morandini, *Chem Rev.* **1987**, *87*, 761−778. − [28b] G. Consiglio, F. Morandini, *Inorg. Chim. Acta* **1987**, *127*, 79−85.
[29] [29a] S. Abott, S. G. Davies, P. Warner, *J. Organomet. Chem.* **1983**, *246*, C65−C68. − [29b] R. M. Bullock, *J. Chem. Soc., Chem. Commun.* **1989**, 165−167. − [29c] M. I. Bruce, G. A. Koutsantonis, *Aust. J. Chem.* **1991**, *44*, 207−217.
[30] M. I. Bruce, R. C. Wallis, *Aust. J. Chem.* **1979**, *32*, 1471−1485.
[31] WIN-DYNAMICS 1.0 Release 951220, *NMR Dynamic Spectra Simulation and Iteration*, Bruker-Fanzen Analytik GmbH and K. Ill′yasow, O. Nedopekin, Bremen, Germany.
[32] *Organikum*, Deutscher Verlag der Wissenschaften, Berlin, **1990**.
[33] "Collect" data collection software, Nonius, **1998**.
[34] [34a] G. M. Sheldrick, *SHELXS-97, Program for Crystal Structure Solution*, University of Göttingen, **1997**. − [34b] G. M. Sheldrick, *SHELXL-97, Program for Crystal Structure Refinement,* University of Göttingen, **1997**. − [34c] *International Tables for X-ray Crystallography*, vol. 4, Kynoch Press, Birmingham, U.K., **1974**.
[35] L. Zsolnai, G. Huttner, *XPMA, http://www.rzuser.uni-heidelberg.de/v54/xpm.html,* Universität Heidelberg, **1994**.
[36] A. M. Z. Slawin, D. J. Williams, J. Crosby, J. A. Ramsden, C. White, *J. Chem. Soc., Dalton Trans.* **1988**, 2491−2494.

Received June 23, 1999
[I99229]